FT-NMR AND RAMAN SPECTROSCOPIC STUDIES OF MOLECULAR DYNAMICS IN LIQUIDS

DISSERTATION

Presented to the Graduate Council of the
University of North Texas in Partial
Fulfillment of the Requirements

For the Degree of

DOCTOR OF PHILOSOPHY

By

Kuen-Shian Wang, B.E., M.S.

Denton, Texas

December, 1993

FT-NMR AND RAMAN SPECTROSCOPIC STUDIES OF MOLECULAR DYNAMICS IN LIQUIDS

DISSERTATION

Presented to the Graduate Council of the
University of North Texas in Partial
Fulfillment of the Requirements

For the Degree of

DOCTOR OF PHILOSOPHY

By

Kuen-Shian Wang, B.E., M.S.

Denton, Texas

December, 1993

Wang, Kuen-Shian, FT-NMR and Raman Spectroscopic Studies of Molecular Dynamics in Liquids. Doctor of Philosophy (Chemistry), December, 1993, 126 pp., 12 tables, 9 figures, reference list, 118 titles.

NMR relaxation and Raman lineshape analysis are well known methods for the study of molecular reorientational dynamics in liquids. The combination of these two methods provides another approach to tackle the characterization of molecular dynamics in liquids.

Investigations presented here include (1) NMR relaxation study of polycyclic compounds in solution, (2) the study of nitromethane reorientational dynamics using the NMR and Raman methods, and (3) Raman lineshape analysis of reorientation hexafluorobenzene/benzene mixtures.

^{13}C dipole-dipole relaxation times and NOE enhancements effect of five "cage" compounds in solution were measured to derive diffusion constants ($D_{\parallel}$ and $D_{\perp}$) of each compound in $CHCl_3$ as a function of temperature. Results showed that substitution affected $D_{\perp}$ but had an insignificant effect on $D_{\parallel}$. Intermolecular association was important in determining diffusion constants.

Raman degenerate vibration bandshapes (E modes) in C_{3v} molecules were routinely used to extract $D_{\parallel}$ in systems with

methyl rotors. The Raman bandshapes of the ν_1 and ν_7 vibrations in nitromethane-d_3 were studied as a function of temperature in liquid phase to test the applicability of this method to molecules with lower symmetry. $T_1(^2D)$'s were obtained to derive $D_\parallel$ of CD_3NO_2. $D_\parallel$'s from Raman bandshapes were greater than those from $T_1(^2D)$. Hydrogen bond interaction may be the main contribution of the band broadening and result in greater $D_\parallel$(Raman) than $D_\parallel(^2H)$.

To better characterize the reorientational dynamics in hexafluorobenzene/benzene (HFB/B) mixtures, the Raman bandshapes of a_{1g} and e_{2g} vibrations in both molecules were measured as a function of the HFB mole fraction (χ_{HFB}) and the diffusion constants for each species as a function of χ_{HFB} were derived. $D_\perp$(B) decreased with increasing solution viscosity in agreement with hydrodynamical prediction; $D_\perp$(HFB) showed the opposite trend, indicative of slowed tumbling of the HFB due to complexation. The $D_\parallel$(B)'s remained independent of concentration, whereas the $D_\parallel$(HFB) decreased at higher χ(HFB).

TABLE OF CONTENTS

LIST OF TABLES

LIST OF ILLUSTRATIONS

CHAPTER I

GENERAL INTRODUCTION

A. Molecular Reorientational Dynamics in Liquids

The rotational motion of molecules in the gas phase is well represented by the equipartition of energy theorem and the laws of statistical mechanics, both of which are premised on the view that the molecules move independently of one another. In the liquid phase, due to strong intermolecular interaction, the situation is rather more complicated than in the gas phase. The difficulties of understanding liquid phase behavior arise from the fact that, in liquids, the molecules are undergoing rapid, erratic movements and frequent collisions. Small intermolecular separations make the liquid system very susceptible to the forces present between molecules. These intermolecular forces, which are molecule specific, play a significant role in molecular dynamics. One macroscopic manifestation of these unique liquid phase characteristics is the bulk viscosity of the system. For most molecules in the liquid phase, the rotational rate depends upon the viscosity and is independent of the moment of inertia, indicating that intermolecular frictional forces are the dominant factors. These physical interactions between

molecules in liquids have been a persistent challenge to chemists. In the past, several models have been proposed to account for the dynamic behavior of liquids. One that has received tremendous attention is the rotational diffusional model.

B. Theory of Rotational Diffusion

1. Reorientation

The diffusion concept originated in an attempt to describe the spontaneous translational motion of small particles and carries with it implications of a continuous and retarding force. The rotational diffusion model of a liquid views the reorientational motion of a molecule as being impeded by a viscosity-related frictional force where continuous motion is implied. If the rotational friction coefficient operating at the surface of the molecule, regarded as a sphere, is represented by the macroscopic viscosity, η, then the rotational friction coefficient has the Stokes value[1]

$$\epsilon = 8\pi a^3 \eta \qquad (1)$$

and the rotational diffusion rate is given by[2]

$$D_{rot} = kT/\epsilon = kT/8\pi a^3 \eta \qquad (2)$$

where k is Boltzmann's constant, T is the temperature, ϵ is

the rotational friction coefficient, a is the hydrodynamic radius of particle, and η is the shear viscosity of the medium.

In the hydrodynamical view of molecules rotating in a continuous fluid, it is assumed that the molecule undergoes small, random jumps about its three axes, each of which is characterized by a rotational diffusion constant (D_i, i = x, y, z). The root-mean-square (r.m.s.) angle of rotation during a time interval, Δt, is given by:[3,4]

$$\langle \Delta\theta \rangle_{rms} = \langle \Delta\theta_i^2 \rangle^{1/2} = \langle 2D_i \Delta t \rangle^{1/2} \tag{3}$$

The value of Δt required for $\langle \Delta\theta \rangle_{rms}$ to reach one radian is defined as the correlation time, τ_θ.

For symmetric-top molecules with the z-axis chosen along the principal axis, the reorientational diffusion constants characterize the reorientation as

$$D_x = D_y = D_\perp \tag{4}$$

and

$$D_z = D_\parallel \tag{5}$$

For totally asymmetrical molecules there are three different diffusion constants.

2. Rotational Diffusion and Diffusion Constants

The major objective of liquid-phase molecular dynamics

studies is to determine the dynamic parameters, using the concept of rotational diffusion, which characterize the reorientational motions of molecules.

Molecular reorientation in the liquid phase is usually characterized by either rotational diffusion constants, D's, or reorientational correlation times, τ's. The molecular reorientation correlation time, τ_c, is approximately the time required for a molecule or a relaxation vector to rotate one radian. For a spherical top molecule, whose motion is isotropic in nature, a single diffusion constant or a single τ is needed to describe its reorientational motion. Symmetric-top molecules, which experience anisotropic motion, require two diffusion constants ($D_\parallel$ and $D_\perp$) to characterize the reorientational motion. $D_\parallel$ and $D_\perp$ represent spinning and tumbling rates respectively. For a nonspherical top molecule, which may reorient at different rates about different molecular axes, the effective correlation time is a complicated function of many external and internal molecular motions. In principle, by measuring τ_c for several different nuclei in a molecule, it is possible to determine the individual components of the rotational diffusion tensor for a molecule experiencing anisotropic motion.[5-7] Relaxation measurements of nuclei with various orientations of the nuclear vector in the molecule must be combined to yield information on the molecular motion.

3. Correlation Function and Correlation Time

The reorientational correlation function of a single rigid molecule is a measure of the degree of correlation between the orientation of a molecule at time **t** and the same molecule at time 0. It answers the question about how well a molecule in a condensed phase remembers where it was pointing at a time **t** earlier.

Varying with the experimental techniques, the correlation functions for different motions can be used to measure related molecular properties. NMR and Raman spectroscopies are two of these spectroscopic methods. Molecular rotational motions are known to have an influence on both Raman scattering of light and nuclear spin relaxation. NMR spectroscopy concerns the property of spin relaxation and the motions involved are molecular reorientations. In nuclear spin relaxation, molecular rotation is coupled to the nuclear spin by a number of mechanisms. By measuring the dynamics behavior of the spin, it is possible to draw conclusions about molecular rotation. Raman spectroscopy concerns the property of polarizability and the motions involved are also molecular reorientations. In Raman scattering, the rotation and vibration of a molecule modulate its polarizability and thus the frequency distribution of the scattered light contains information about the rotational motion.

C. Theoretical Reorientational Diffusion Models

In an attempt to predict liquid-phase molecular rotational diffusion constants which characterize the molecular reorientation in liquid systems, several diffusion models have been developed in past years. It may be possible to give *a priori* predictions[8] of the rates of molecular rotation of symmetric top molecules in solution based on these models.

1. The Stokes-Einstein-Debye (SED) Model

The first model attempting to describe the resistance to the rotation of a macroscopic sphere rotating in a viscous liquid was developed by Stokes[1] in 1856. The friction constant is given by

$$\epsilon = \text{torque/angular momentum} = 8\pi a^3 \eta \qquad (1)$$

where a is the radius of the molecule and η is the viscosity of the medium.

A extended application of the above model was proposed by Einstein and Debye. In the case of spherical top molecules, the rotational diffusion constant (D_o) is given by[2]

$$D_o = kT/\epsilon \qquad (2)$$

The resulting expression becomes $D_o = (kT/8\pi a^3 \eta)$.

From the experimental results of many NMR relaxation studies, it has been concluded that the actual rotational rates are much faster than rates predicted from the SED model. Such results indicate that the frictional restraint must be lower than that represented by the Stoke's coefficient. This discrepancy suggests that the bulk viscosity, η, does not appropriately represent the effective viscosity at the surface of the molecule.

2. The Stick (Perrin) Model

The earliest hydrodynamic theory of anisotropic reorientation was developed by Perrin,[9] who extended the SED 'stick' model to rotating nonspherical molecules in a viscous, continuous medium. Perrin's stick model assumes that the solvent sticks to the surface of the molecule, thus creating a viscous drag, which retards its rotation. Perrin solved the Navier-Stokes equation[1] to obtain diffusion constants, given by:

$$D_i = (1/f_i)D_o = (1/f_i)(kT/8\pi r^3\eta) \qquad (6)$$

In this equation, $D_i = D_\perp$ or $D_\parallel$, $f_i = f_\perp$ or $f_\parallel$, D_o is the original SED isotropic diffusion constant; k is Boltzman's constant; T is the temperature in kelvin; η is the viscosity; and $r = (ab^2)^{1/3}$ is the mean radius of the particle.[10] The correlation factors, $f_\perp$ and $f_\parallel$, are dependent on the axial ratio, $\rho = b/a$, and on whether the

rotor is prolate or oblate in shape.

Like the SED model for spherical molecules, Perrin's stick model predicts rotational diffusion constants an order of magnitude smaller than the experimental values[11] and proves to be inadequate for small-to-medium size molecules.

3. The Free Rotor (FR) Model

The free rotor model assumes that the surrounding solvent does not stick at all to the rotating molecule. For spherical molecules, there is no retarding friction and the molecule rotates freely (as in gas phase) at a rate controlled by its moment of inertia. The diffusion constant is given by[12]

$$(D)_{FR} = [6\tau_{FR}]^{-1} \tag{7}$$

where τ_{FR} is the time for a "free rotor" to rotate 41°,

$$\tau_{FR} = 2\pi(41/260)(I/kT)^{1/2} \tag{8}$$

and I is the molecular moment of inertia, k is Boltzmann's constant, and T is the temperature in Kelvin.

4. The Slip (HZ) Model

As noted, the original Perrin 'stick' model of anisotropic reorientation in liquids[9] yields calculated diffusion constants, $D_{\perp}$ and $D_{\parallel}$, which are an order of

magnitude smaller than experimental values. To overcome this deficiency, Hu and Zwanzig[13] introduced an alternative 'slip' theory for prolate and oblate symmetric tops, in which solvent molecules are assumed to glide smoothly past the surface of the solute and the solute's resistance to reorientation is caused by the displacement of solvent as the molecule rotates. In the HZ slip model limit, a spherical molecule experiences no opposing force and is expected to rotate as rapidly in solution as does a free rotor in the gas phase. A 'slip' boundary condition (zero tangential stress) is probably more realistic for rotation on a molecular scale.

For the rotation of a sphere or that parallel to the unique axis of a symmetric top ($D_{\parallel}$), this condition implies vanishing friction and, therefore, the molecule can be treated as a "free rotor". The rotation perpendicular to the top axis ($D_{\perp}$) is retarded since it requires displacement of solvent molecules. Hu and Zwanzig[13] solved the Navier-Stokes equation numerically, by using the slip boundary condition, and obtained the perpendicular diffusion constant, which is given by the following expression:

$$D_{\perp} = (1/f_{HZ})(kT/8\pi b^3\eta) \qquad (9)$$

where b is the largest semi-axis length, f_{HZ} is a numerical factor dependent on the axial ratio and on whether the

molecule is prolate or oblate. The Hu-Zwanzig factor, f_{HZ}, may be obtained from the reduced friction coefficients ($f_{HZ} = \xi^*/8$) in Table I of their article.[13]

5. The Microviscosity (MV) Model

In order to account for the discrepancy encountered with the purely 'stick' treatment, Gierer and Wirtz[14] (GW) introduced a rotational microviscosity correction factor into the SED model. The rotational microviscosity correlation factor, f_{GW}, is given by

$$f_{GW} = [6(a_s/a) + (1 + a_s/a)^{-3}]^{-1} \qquad (10)$$

where a_s/a is the ratio of solvent to solute radius. When $a_s/a >> 1$, it corresponds to the "slip" boundary condition, in which the rotating molecule slips through the solvent without retarding forces ($\epsilon = 0$) and yields the same results as the slip model. When $a_s/a << 1$, it corresponds to the "stick" boundary condition, in which the rotating molecule experiences a retarding force ($\epsilon = 8\pi a^3\eta$) and generates the results obtained with the stick model. In pure liquids, $a_s/a = 1$, which gives a microviscosity factor, $f_{GW} = 0.16$, and represents a friction coefficient with 16% of the stick value.

6. The Hynes-Kapral-Weinberg (HKW) Model

Hynes, Kapral and Weinberg[15,16] introduced a new

formalism, in which they incorporate a slip coefficient, β, whose magnitude is dependent on the frictional torque exerted by the solvent. The HKW model provides a general description for the reorientational behavior of molecules in liquids and the theory allows for the fact that rotation actually lies between the "stick" and "slip" limits. The magnitude of β indicates the degree of coupling between the particle's rotation and the solvent continuum. $\beta = 0$ corresponds to the slip boundary condition, whereas the hydrodynamic stick limit is approached as $\beta \rightarrow \infty$. They developed an expression for the rotational diffusion constant and also employed the Enskog collision theory[16] to obtain an equation for the approximate calculation of β.

The extended HKW model demonstrates considerable promise in narrowing the gap between calculated and experimental rotational diffusion constants.[17-21] The HKW model was originally developed for spherical particles. Tanabe[22,23] modified the HKW equations (model) in order to calculate the diffusion constants ($D_{\parallel}$ and $D_{\perp}$) of symmetric-top molecules:

$$D_{\perp} = (1/f_{\perp})\ D_o[1 + (3\eta/\beta + \alpha_{\perp}\eta)] \qquad (11)$$

$$D_{\parallel} = (1/f_{\parallel})D_o[1 + (3\eta/\beta)] \qquad (12)$$

where $f_{\perp}$ and $f_{\parallel}$ are the Perrin coefficients[9] and D_o is the

SED diffusion constant [$D_o = kT/(8\pi r^3\eta)$]. Therefore, in the stick limit ($\beta \rightarrow \infty$), the above expressions reduce to the Perrin results for $D_\parallel$ and $D_\perp$. In addition, $D_\parallel$ diverges in the slip limit ($\beta = \phi$). The quantity $\alpha_\perp$ in eq. 11 can be calculated by the relation

$$\rho^2/f_{HZ} = (1/f_\perp)[1 + (3/\alpha_\perp)] \tag{13}$$

The slip coefficient, β, may be estimated from the Enskog theory as[24]

$$\beta = [2\kappa/(\kappa + 1)](2\mu_{12}kT/\pi)^{1/2}\rho_2 g_{12}(\sigma_{12}) \tag{14}$$

where μ_{12} is the reduced mass of the solute-solvent pair; σ_{12} is the mean diameter, $(\sigma_1 + \sigma_2)/2$; and ρ_{12} is the solvent's number density. The radial distribution function, $g_{12}(\sigma_{12})$, can be derived by the methods presented in one of Tanabe's articles.[25] Finally, $\kappa = I_{avg}/mr^2$, where $I_{avg} = (2I_x + I_z)/3$ and m is the molecular mass.

CHAPTER REFERENCES

1. Stokes, K. Trans. Cambridge Phil. Soc., **1856**, 9, 5.

2. Debye, P. Polar Molecules; Dover, New York, 1928.

3. Wasylishen, R. E.; Pettitt, B. A.; Danchura, W. Canad. J. Chem. **1977**, 55, 3602.

4. Youngren, G. K.; Acrivos, A. J. Chem. Phys. **1975**, 63, 3846.

5. Sandhu, H. S. J. Mag. Reson., **1978**, 29, 563.

6. Sandhu, H. S. J. Mag. Reson., **1977**, 26, 7.

7. Sandhu, H. S. J. Mag. Reson., **1976**, 21, 7.

8. (a) Chen, A. F. T.; Wang, S. P.; Schwartz, M. Magn. Reson. Chem. **1988**, 26, 675. (b) Rodriguez, A. A.; Chen, A. F. T.; Schwartz, M. J. Mol. Liq. **1988**, 37, 117.

9. Perrin, E. J. Phys. Radium, **1934**, 5, 497.

10. In a symmetric top molecule, the semi-axis lengths of the volume ellipsoid are given by a, b, and c, where b and c are equal.

11. Martin, M. L.; Martin, G. J.; Delpuech, J. J. Practical NMR Spectroscopy; Heyden: London, **1980**; Chapter 7.

12. Boere, R. T.; Kidd, R. G. Ann. Rept. NMR Spect., **1982**, 13, 319.

13. Hu, C.-M.; Zwanzig, R. J. Chem. Phys., **1976**, 60, 4354.

14. Gierer, A.; Wirtz, K. Zeit. Naturforsch. **1953**, A8, 523.

15. Hynes, J. T.; Kapral, R.; Weinberg, M. Chem. Phys. Letters, **1977**, 46, 463.

16. Hynes, J. T.; Kapral, R.; Weinberg, M. J. Chem. Phys., **1978**, 69, 2725.

17. Tanabe, K. Chem. Phys., **1978**, 31, 319.

18. Tanabe, K.; Hiraishi, J. Mol. Phys., **1980**, 39, 493.

19. Wang, S. P.; Chen, A. F. T.; Schwartz, M. Mol. Phys., **1988**, 65, 689.

20. Yuan, P.; Chen, A. F. T.; Schwartz, M. J. Raman Spectrosc., **1989**, 20, 27.

21. Chen, A. F. T.; Wang, S. P.; Schwartz, M. Magn. Reson. Chem., **1988**, 26, 675.

22. Berne, B. J.; Harp, G. D. Adv. Chem. Phys., **1970**, 17, 63.

23. Berne, B. J. Physical Chemistry: An Advanced Treaties; Eyring, H., Henderson, D., Jost, W. ed,; Academic: New York, 1971, Vol. VIII B, p. 539.

24. (a) Hynes, J. T.; Kapral, R.; Weinberg, M. Chem. Phys. Lett. **1977**, 46, 463. (b) Hynes, J. T.; Kapral, R.; Weinberg, M. J. Chem. Phys. **1978**, 69, 2725.

25. Tanabe, K. Chem. Phys. **1978**, 38, 125.

CHAPTER II

NUCLEAR MAGNETIC RESONANCE RELAXATION AND MOLECULAR DYNAMICS

Since the pioneering work of Bloembergen, Purcell, and Pound[1], NMR has been proved to be an extremely powerful tool in the study of molecular motion of materials in the condensed phase. Not only is this technique useful in the study of the dynamics of the translational diffusion of atoms and molecules (mass flow), but also it is useful in the study of molecular-reorientation processes when mass flow is absent. Because of much activity in the development of this technique, most of the theoretical problems concerning NMR spectroscopy have been clarified. This allows researchers to interpret experimental results on a firm theoretical ground and permits unambiguous conclusions about the nature of molecular motion.

A. Basic Theory

The concept of NMR was originally developed in the classic studies of Purcell, Torrey, and Pound[2] and Bloch, Hansen, and Packard,[3] who independently observed the first NMR signals. Since then, the theory has been considerably modified and extended by a number of authors.[4-8]

NMR spectroscopy is concerned with the atomic nuclei in a molecule. Most nuclei have a spin angular momentum, which

is expressed in terms of the maximum observable component ofthe nuclear spin (i.e., the spin quantum number I). When applying a uniform magnetic field H_o (assumed to be in the Z direction), the spin degeneracy is removed, a nucleus of spin I will have 2I + 1 energy levels (the values can be 0, ±1/2, ±1, ..., etc.) equally separated by

$$\Delta E = \mu H_o / I \tag{15}$$

where H_o is the static magnetic field, and μ, the nuclear magnetic moment, which is proportional to I, is given by[5]

$$\mu = \gamma \hbar I \tag{16}$$

where γ is the magnetogyric ratio, which is a constant for a given nucleus, and $\hbar = h/2\pi$, where h is Plank's constant. The energy of each spin state of the nucleus in the magnetic field, by combining the above two equations, can be expressed as

$$\Delta E = \gamma \hbar H_o \tag{17}$$

According to the Bohr relation, the frequency of radiation can induce transitions between the different spin states. Such transitions then give rise to a net absorption of energy, which is

$$h\nu = \Delta E = \gamma \hbar H_o \tag{18}$$

where ν is the Larmor frequency, $\nu = \gamma H_o/(2\pi)$ in Hz or $\omega = 2\pi\nu = \gamma H_o$ in radian per second. The equation of motion of the nuclear magnetic moment can be written as $d\mu/dt = \gamma\mu x H_o$. Such an equation describes a precession of the μ vector about H_o, as shown by Figure 1(a), at the Larmor angular velocity, $\omega = -\gamma H_o$. Figure 1(b) shows the precession of an ensemble of nuclei with spin I = 1/2.

When an ensemble of nuclei is placed in a magnetic field, after a sufficient amount of time, a net magnetization M_o in the field direction will result. This can be described by Curie's law[4]

$$M_o = N\gamma^2\hbar I(I + 1)H_o/(3kT) \tag{19}$$

where N is the density of nuclei. This magnetization is due to the preferential population of the lower energy level according to Boltzmann's distribution.

As described by Boltzmann's distribution, there is an excess of nuclei in the lower energy state at equilibrium, which is established by means of specific relaxation processes. If an RF magnetic field, H_1, is applied after equilibrium is reached, the nuclei absorb energy, and the populations of the two spin states tend to equalize.

When the magnetization is perturbed from its

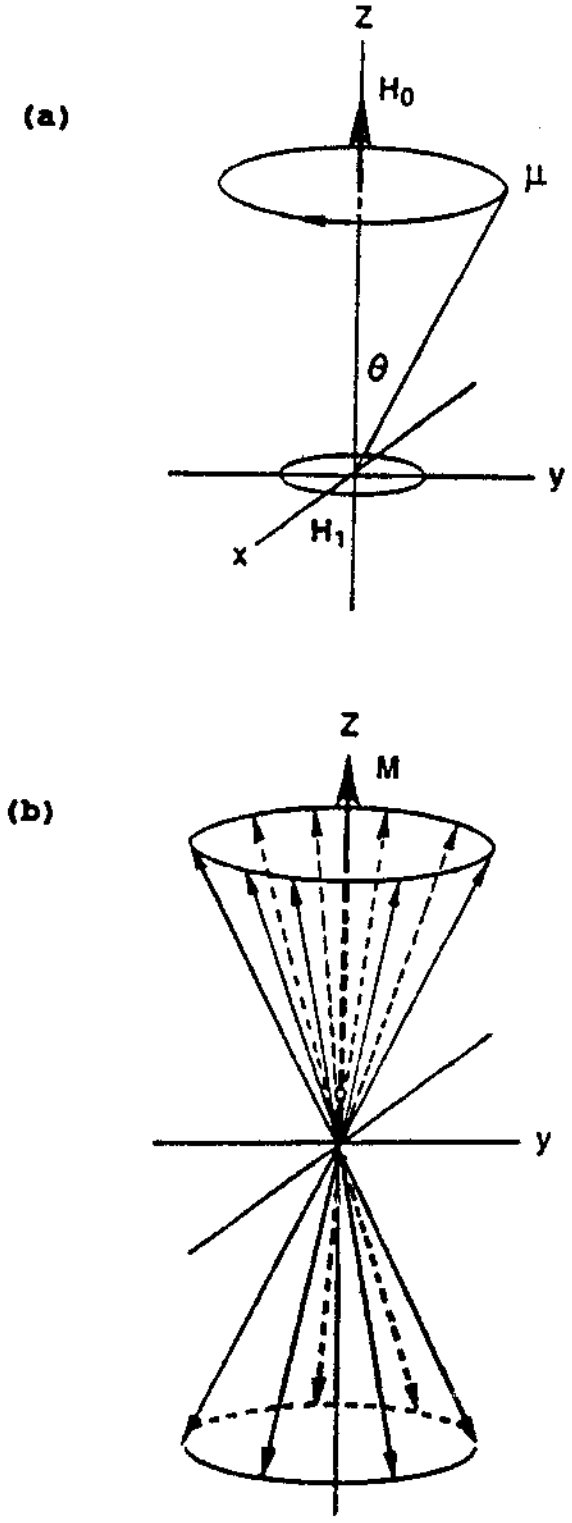

Figure 1. Precession of nuclei in a magnetic field.
(a) Pression of μ about H_o.
(b) Pression of an ensemble of nuclei with I = 1/2.

equilibrium value M_o by applying an RF magnetic field H_1 perpendicular to H_o, the interaction between the magnetization and the magnetic field will exert a torque on the nonequilibrium magnetization which tends to align it parallel to the field. Since this torque alters only the component of angular momentum perpendicular to H_o and μ, the net result leads to a rotation of the direction of μ in a cone with its axis along H_o. Such rotation is called Larmor precession and represented by[9]

$$d\mathbf{M}/dt = \gamma\ (\mathbf{M} \times \mathbf{H}_{eff}) \qquad (20)$$

where $\mathbf{M}$ is the magnetization and $\mathbf{H}_{eff}$ is the effective field strength and $H_{eff} = H_{o,z} + H_{1,x}$.
when there is no interaction between the spins or with their surroundings.

Eventually, when H_1 is removed, the system will return to the former equilibrium distribution appropriate to H_o through the same energy relaxation phenomena. The excess nuclear population is then restored to the lower energy level, and the energy previously absorbed by the spin system is transferred to the "lattice" (its surroundings) by a first-order relaxation process, giving rise to what is called spin-lattice relaxation.[4]

In order to observe more precisely the motion of the magnetization vector in the presence of the magnetic fields

H_o and H_1, it is important to view M from a reference frame rotating at the Larmor frequency. Therefore, the magnetization appears to be a constant vector with components both parallel (M_z) and perpendicular (M_x, M_y) to the applied field. Both average values of magnetization (M_x and M_y) in the x and y directions are zero in the equilibrium state. Resonance will occur if an exciting field H_1 is applied exactly at the Larmor frequencies of the nuclei. When the applied field H_1 is removed, magnetization will return to its equilibrium state M_o by two types of relaxation process. The z component, M_z, will return to its equilibrium state by spin-lattice relaxation

$$dM_z/dt = -(M_z - M_o)/T_1 \qquad (21)$$

where T_1 is a first order time constant, which characterizes the behavior of the z component of the macroscopic nuclear magnetization, M_z, in a static magnetic field, B_o. The explanation of the occurrence of spin-lattice relaxation is that it occurs via transitions which are stimulated by components of the local magnetic field of a particular nucleus which fluctuate at its Larmor frequency. These fluctuations in the local magnetic field result from the Brownian motion of the two interacting nuclei.

The nonequilibrium component of magnetization, M_x or M_y, is also dependent on the relaxation and its environment

and is zero at equilibrium. The relaxation is also characterized by a first order rate with exponential decay time, T_2, which is the time taken for the magnetization, M_x, to decay to 1/e of its initial value. T_2 is known as the spin-spin relaxation time and can be expressed as

$$dM_{xy}/dT = - M_{xy}/T_2 \qquad (22)$$

Spin-spin relaxation also occurs through local magnetic fields. When a nucleus undergoes a transition from one spin state to another, the local magnetic field changes at the same frequency to induce a transition in a second nucleus. If a second nucleus of the same type with opposite spin state is close by, then energy exchange will occur between these two nuclei. Such a process does not change the total system energy but affects the life time of the excited state. Therefore, spin-spin relaxation is an entropy effect, whereas spin-lattice relaxation is an energy effect. In most of the cases T_2 is always shorter than T_1 because of two effects. The first effect is due to static dipole fields orienting from other nuclei with the sample, which only interact with M_x or M_y. The second effect arises from inhomogeneities in the magnetic field due to instrumental imperfection.

As many as five different independent mechanisms may contribute to the total relaxation process. The following

sections of this chapter are brief review and discussions of these relaxation mechanisms.

B. Relaxation Mechanisms

The fact that the nuclear magnetic resonance relaxation parameters depend on the exact movement through the fluctuating local magnetic fields provides a unique opportunity to study dynamic interactions in solution. When the nuclei have absorbed radiation and have been excited to the upper energy level, there are many ways to return to the lower energy state by exchanging energy with their environment. This energy exchanging process is called spin-lattice relaxation. The efficiency of this energy exchanging process is characterized by the relaxation time, T_1, or by the relaxation rate, $R_1 = 1/T_1$. The spin-lattice relaxation time characterizes the time required for a perturbed system of nuclei to return to an equilibrium condition. A larger value of T_1 means an inefficient relaxation process. There are five types of interaction which cause the nuclei system to relax its energy, namely, nuclear magnetic dipole-dipole interaction, nuclear electric quadrupole interaction, spin-rotation interaction, chemical shift anisotropy, and scalar coupling effects. The experimental relaxation rate is usually considered to be the summation of the specific rates of all the relaxation mechanisms involved. In principle, all the interactions may

contribute to the overall relaxation process. However, in many cases only one or two of the numerous possible mechanisms predominate and a quantitative interpretation can be achieved.

1. Dipole-Dipole (DD) Relaxation

The major source of the nuclear relaxation for nuclei with a spin quantum number equal to 1/2 is via dipole-dipole interaction. Considering the relaxation of a nucleus **I** by another nucleus **S**, due to random motions in the sample, spins **I** and **S** will change orientation and position relative to each other and spin **I** will experience a fluctuating magnetic field of magnitude H_{loc}. The local field (H_{loc}^{DD}) generated at **I** by **S** is given by the classical equation[10]

$$H_{loc}^{DD} = \pm \mu_S(3\cos^2\theta - 1)r_{IS}^{-3} \qquad (23)$$

where μ_S is the magnetic moment of **S**, θ is the angle between the static field and the axis through **I** and **S**, and r_{IS} is the distance between **I** and **S**.[10] As the molecule tumbles in solution under the influence of Brownian motion, this field fluctuates in magnitude and direction.

Just as a precessing nuclear moment can interact with a coherently applied RF magnetic field, so can it interact with the component of a molecular magnetic field precesses at the Larmor frequency.[11] Therefore, the relaxation

arising from the fluctuating field will depend on the molecular motion, magnitudes of the nuclear moments, and the distance between the interacting nuclei. A detailed treatment of the relaxation process shows that[12]

$$\frac{1}{T_{1DD}} = \frac{\gamma_i^2\gamma_j^2 h^2 S(S+1)}{30\pi^2 r_{ij}^6} \times \left[\frac{3\tau_c}{1+\tau_c^2\omega_I^2} + \frac{\tau_c}{1+\tau_c^2(\omega_I-\omega_S)^2} + \frac{6\tau_c}{1+\tau_c^2(\omega_I+\omega_S)^2}\right] \tag{24}$$

where γ_i and γ_j are the magnetogyric ratios for nuclei with nuclear spin I and S, respectively; τ_c is the reorientational correlation time; ω_I and ω_s are the Larmor frequencies for nuclear spins I and S. The rapid random motion of molecules will lead to a very short τ_c. When the extreme narrowing condition, $\tau_c\omega_o << 1$, is satisfied, the above equation can be simplified to

$$R_{1,DD} = 1/T_{1,DD} = (4/3)n_s[\gamma^2{}_i\gamma^2{}_j\hbar^2 S(S+1)/r^6{}_{ij}]\tau_c \tag{25}$$

There are three things revealed by equation (25): First, because the local field depends on μ_s, the nucleus with the largest nuclear magnetic moment (such as proton) will be the most powerful source of internuclear relaxation. Second, due to inverse sixth power dependence on the interdipole distance, dipole-dipole relaxation is a very

short-range effect. The third one is that dipole-dipole relaxation is magnetic field independent and temperature dependent. The correlation time remains invariant in different magnetic fields but will change as the temperature changes. At high temperatures, τ_c is shorter (faster motion), and the efficiency of dipole-dipole interactions is lowered. Under this situation, a longer $T_{1,DD}$ will result.

The relaxation of the spin dipole is caused both by other spins on the same molecule (intramolecular) and on different molecules (intermolecular). When the nuclear spin is located on the interior of the molecule, intermolecular relaxation is negligible. When studying relaxation times, the intermolecular contribution is usually eliminated by dissolving the solute in a solvent which does not have significant nuclear magnetic moment. Once the relaxation times have been determined by experimentation, they can provide information about the correlation times of spin-spin vectors in the molecule, which can be used to characterize the molecular reorientation.

2. Quadrupole Relaxation (QR)

Nuclei with spin quantum number (I) of 1/2 have a spherical charge distribution. Nuclei with a spin quantum number greater than 1/2, whose charge distribution is nonspherical and have a quadrupole moment Q,[13] will undergo a very efficient relaxation process by interacting with a fluctuating electric field opposed to a magnetic field. In

the liquid phase, the quadrupole mechanism is usually four or five orders of magnitude more effective than other mechanisms in promoting relaxation, and where present, accounts for essentially all of the relaxation.

In the simplified case of extreme narrowing conditions, the quadrupole relaxation rate can be given by[14]

$$R_{1,QR} = 1/T_{1,QR} = 3/125(e^2qQ/h)^2[1 + (\eta^2/3)]\tau_c \qquad (26)$$

where e^2qQ/h is the electric Quadrupole Coupling Constant (QCC), which is made up of the nuclear quadrupole moment, Q, the electric field gradient, **q**, and the fundamental constants e and h. τ_c is the correlation time for molecular reorientation, and η is the asymmetry factor. By measuring $T_{1,QR}$, one can obtain the QCC, which measures the asymmetry of electronic charge distribution around the nucleus. Since $T_{1,QR}$ depends upon the reorientational correlation time, its relation to temperature is the same as that for $T_{1,DD}$.

3. Spin-Rotation Relaxation (SR)

Apart from the dipole-dipole (DD) mechanism, it is well known that the contribution from the spin-rotation (SR) interaction is important for ^{13}C relaxation, especially for small and rapidly tumbling molecules. Spin-rotation relaxation arises from magnetic fields generated at a nucleus by the motion of a molecular magnetic moment which arises from the electron distribution in a molecule.

Consider a rotating molecule with a moment of inertia I. Any electron in the molecule undergoing such rotation will generate a local magnetic field at the nucleus because it behaves like a circulating electric current. Molecular collisions, causing changes in both direction and rotational rate, will modulate this field and provide a relaxation process. For molecules undergoing diffusional reorientation, the spin-rotation relaxation rate for a symmetric top molecule[15] can be expressed by

$$1/T_{1,SR} = (8kT/3\pi^2h^2)[I_{\parallel}C_{\perp}^2(\tau_j)_{\parallel} + 2I_{\perp}C_{\perp}^2(\tau_j)_{\perp}] \qquad (27)$$

where $I_{\parallel}$ and $I_{\perp}$ are components of the inertia tensor and $C_{\parallel}$ and $C_{\perp}$ are components of the spin-rotation tensor with respect to the symmetry axis. The terms $(\tau_j)_{\parallel}$ and $(\tau_j)_{\perp}$ are the angular momentum correlation times about the appropriate axes.

Symmetric molecules with little or no intermolecular interaction will be affected by SR relaxation, because they will have relatively larger angular velocities. For spherical molecules, in which $I_{\parallel} = I_{\perp} = I$ and $(\tau_j)_{\parallel} = (\tau_j)_{\perp} = \tau_j$, the equation (27) can be written as

$$1/T_{1,SR} = (2\pi IkT/h^2)(C_{eff})^2\tau_J \qquad (28)$$

where C_{eff} is the average component of the spin-rotation

tensor and τ_J is the angular momentum correlation time, which is a measure of the residence time of a molecule in any given angular momentum state. For spherical molecules undergoing small step diffusion, τ_J is related to the molecular reorientation correlation time τ_c by the Hubbard relationship[16]

$$\tau_c * \tau_J = I/(6kT) \tag{29}$$

It is that τ_J and τ_c are inversely related to each other. Within this diffusion concept, τ_J is the time between collision that change the angular momentum and is required to be much shorter than τ_c ($\tau_J << \tau_c$). The best way to judge if the spin-rotation relaxation is dominant is to see if T_1 decreases as temperature increases since τ_c becomes shorter, and τ_J becomes longer, as the sample temperature increases. At low temperatures, $R_{1,SR}$ is inefficient and $R_{1,DD}$ is efficient because of the slow molecular motion. As the temperature increases, $R_{1,DD}$ decreases slowly due to decreasing τ_c until $R_{1,DD}$ becomes negligible. At high temperatures, T_1 begins to decrease with temperature, due to the spin-rotation relaxation. In general, spin-rotation interactions are important with nuclei that have a large range of chemical shifts (e.g., ^{19}F, ^{13}C, ^{15}N) because both the chemical shift and the spin-rotation of any given molecule depend on the electron distribution in a molecule.

A distribution which results in large chemical shifts will also lead to large spin-rotation interactions.

4. Chemical Shift Anisotropy (CSA) Relaxation

The magnetic field experienced by a nucleus is not the primary magnetic field but, instead, is modified by the molecule. This modification is expressed in terms of a shielding tensor σ. According to the equation

$$H_{loc} = H_{\phi} - \sigma H_{\phi} = H_{\phi} (1 - \sigma), \tag{30}$$

the local magnetic field, H_{loc}, experienced by a nucleus in a magnetic field is determined by the shielding tensor, which is dependent upon the orientation of the molecule in the magnetic field. Fast molecular motions in liquid state average these values, yielding an average chemical shift, which is expressed as follows:[17,18]

$$\sigma_{avg} = 1/3 \ (\sigma_{xx} + \sigma_{yy} + \sigma_{zz}) \tag{31}$$

For symmetric top molecules, σ is axially symmetric, the equation is reduced to

$$\sigma_{avg} = 1/3 \ (2\sigma_{\perp} + \sigma_{\parallel}) \tag{32}$$

where $\sigma_{xx} = \sigma_{yy} = \sigma_{\perp}$ and $\sigma_{zz} = \sigma_{\parallel}$ refer, respectively, to the shielding perpendicular and parallel to the molecular

symmetry axis. While the molecules are rotating, a fluctuating magnetic field is generated, which can produce a spin-lattice relaxation mechanism. In the extreme narrowing case for axial symmetry, the relaxation rate or relaxation time due to chemical shift anisotropy can be expressed as

$$R_{1,CSA} = (T_{1,CSA})^{-1} = (2/15)\gamma^2 H^2_o (\Delta\sigma)^2 \tau_c \qquad (33)$$

where $\Delta\sigma = \sigma_{\parallel} - \sigma_{\perp}$. In liquid phase, the splitting due to CSA are averaged out by the fast molecular rotation and only a single peak is shown. One way to obtain $\Delta\sigma$ is to measure the NMR splitting in solid phase[19] and liquid crystal.[20]

The relaxation rate due to chemical shift anisotropy increases quadratically with increasing magnetic field, as one may see from equation (33). Chemical shift anisotropy is usually an inefficient mechanism at low magnetic field and is rarely found to contribute significantly to spin relaxation. Some exceptional situations include (1) Experiments performed at very high fields, (2) Heavy molecules with large shielding tensors (σ), and (3) Nuclei with large chemical shift ranges.

5. Scalar Coupling (SC) Relaxation

When a nucleus, **I**, is spin-spin coupled with a second nucleus, **S**, it is possible for **S** to provide a fluctuating magnetic field and cause relaxation of nucleus **I**. This type of relaxation mechanism is called scalar relaxation because

it relies on scalar spin coupling. The field fluctuation iscaused by two sources. One is from the time dependence of the excited state of spin **S**; the other one is from any time dependence of their spin coupling constant, J, resulting from chemical exchange. As **S** relaxes, **I** experiences a magnetic field fluctuation; likewise if J changes, because bond breaking in chemical exchange process, **I** experiences a similar fluctuation.

If the field fluctuations are rapid (in the order of Larmor frequency), the relaxation will be efficient. On condition that $1/T_1^S >> 2\pi J$, T^S_1 is the longitudinal relaxation time of the nucleus S, i.e. if the relaxation rate of nucleus **S** is fast compare to $2\pi J$, no spin coupling will be observed. However, the **I** nucleus to which **S** is spin-coupled experiences a local field that fluctuates at a frequency $1/T_1^S$. This condition is often satisfied for such quadrupolar nuclei as ^{14}N, ^{35}Cl, ^{37}Cl, ^{79}Br, ^{81}Br, ^{127}I, etc. Scalar coupling is frequently found to be a dominant mechanism for transverse relaxation, to the extent where it manifests itself in appreciable line broadening. The relaxation equations of the scalar coupling process for the 'second kind' may be expressed as follow:[14]

$$\frac{1}{T_{1SC}^I} = \frac{8\pi^2 J^2}{3} S(S+1) \left[\frac{T_1^S}{1 + (\omega_I - \omega_S)^2 (T_1^S)^2} \right] \qquad (34)$$

and

$$\frac{1}{T_{2SC}^{I}} = \frac{4\pi^2 J^2}{3} S(S+1)\left[T_1^S + \frac{T_1^S}{1 + (\omega_I - \omega_S)^2 (T_1^S)^2}\right] \qquad (35)$$

where S is the spin of the nucleus **S**, ω_I and ω_S are the Larmor frequencies of the two nuclei, and T^S_1 is the longitudinal relaxation time of the nucleus **S**.

The above two equations show that this mechanism can have very different effect on T_1 and T_2 process. As one may observe that the conditions for scalar spin-lattice relaxation of I to become efficient are rather narrow. The mechanism is field-dependent through the Larmor frequency of the two interacting spins, whose difference occurs in the denominator of the equations (34) and (35). In most common cases $(\omega_I - \omega_S)^2 (T^S_1)^2 >> 1$, so that $T_1{}^S/[1 + (\omega_I - \omega_S)^2 (T_1{}^S)^2]$ becomes very small. Unless this is offset by a very large spin-spin coupling constant, scalar spin-lattice relaxation is negligible. Under this condition, $(1/T_{1,SC}) \approx 0$ and $T^I_{1,SC} \rightarrow \infty$. Equation (35) becomes

$$(1/T^I_{2,SC}) = (4\pi^2/3) S(S+1)\ J^2 T_1{}^S, \qquad (36)$$

which means scalar coupling relaxation contributes only to T_2. In most cases, scalar coupling relaxation does not contribute significantly to the overall T_1. The exceptions occur when the Larmor frequencies of two nuclei are very close. For example, consider ^{13}C-^{81}Br of $CHBr_3$[19] in which

$\gamma(^{13}C) \approx \gamma(^{81}Br)$. In this case scalar coupling doescontribute significantly to T_1 process.[21-25] On the other hand, $(\omega_I - \omega_S)^2(T_1^S)_2 << 1$, due to a very short relaxation time of the coupling nucleus **S**, the quotient $T_1^S/[1 + (\omega_I - \omega_S)^2(T_1^S)^2]$ is still very small and the mechanism is of no importance unless it is balanced by an exceptionally large coupling constant. ^{127}I is an example which is known to give rise very large coupling constant.[26]

C. Separation of Relaxation Mechanisms

The observed (experimental) relaxation rate is the sum of the various mechanisms involved. Each mechanism gives different chemical information. Therefore, in order to acquire the full knowledge from a study of relaxation data, the separate contribution from each mechanism must be resolved. Several methods were proposed for separating the various relaxation mechanisms.[14,27] First, if quadrupolar interaction is present (nucleus with $I > 1/2$ not in a spherical environment), quadrupolar relaxation mechanism is generally predominant over other relaxation mechanisms. Second, since scalar coupling relaxation makes a significant contribution in only very special cases (e.g. in the case of a bromine-bearing carbon), it is normally considered to be absent.

The dipole contribution to the overall relaxation process can be separated from all other relaxation

mechanisms by measuring the nuclear Overhauser enhancement (NOE or η).[12] The NOE is a property whose magnitude is directly proportional to the fraction of the totalrelaxation contributed from the dipole-dipole mechanism. The theoretical maximum NOE can be derived from the magnetogyric ratios or observed when the relaxation is totally dipolar. For proton bearing ^{13}C, the ratio $\eta_{max} = \gamma(H)/2\gamma(^{13}C)$. The experimentally observed NOE is defined as

$$\eta_{exp} = (I_E/I_N) - 1 \tag{38}$$

where I_E is the intensity of the enhanced signal, I_N is the intensity of the non-enhanced signal, and the contribution of the dipole-dipole mechanism can be obtained by

$$T_{1,DD} = T_{1,obs}(\eta_{max}/\eta_{exp}) \tag{39}$$

where $T_{1,obs}$ is the measured spin-lattice relaxation time. When $\eta_{exp} < \eta_{max}$, the presence of a nondipolar relaxation process is indicated. The contribution to the relaxation rate from other processes can be given as

$$T_{1,obs} = (1/T_{1,DD}) + (1/T_{1,other}) \tag{40}$$

Chemical shift anisotropy relaxation is magnetic field dependent as expressed by

$$1/T_{1,CSA} = (2/15)\gamma^2H^2_o(\Delta\sigma)^2\tau_c \tag{33}$$

Experimentally one may measure the overall T_1 value at two different magnetic fields. One may rewrite equation (33) for two different fields H_α and H_β,

$$1/T_1^{\alpha} = a + b(H_\alpha)^2 \tag{41}$$

and

$$1/T_1^{\beta} = a + b(H_\beta)^2 \tag{42}$$

where $a = 1/T_{1,other}$, $b = (2/15)\gamma_c^2(\Delta\sigma)^2\tau_c$. The above two equations can be solved mathematically and $T_{1,CSA}$ can be obtained.

The spin rotation is a mechanism whose T_1 decreases monotonically with temperature. If a nucleus is relaxed partially by spin-rotation, it will show a non-Arrhenius behavior as a function of temperature. This enables spin-rotation to be detected in the presence of other relaxation mechanisms.

D. Correlation Function, Correlation Times, and Diffusion Constants

Molecular motions are coupled to nuclear spins by a number of mechanisms. The relaxation processes of a nucleus are coupled to its surrounding. The energy transfer necessary for the relaxation will only occur if the position vectors determining the instantaneous coupling (magnetic dipolar or electric quadrupolar) between a nucleus and its surroundings are functions of time. Therefore, the

correlation time, τ_c, obtained from a relaxation time measurement is a function of the rotational diffusion constants. The relationship between τ_c and diffusion constants was developed by Huntress[28], Shimizu[29], and Woessner[30] back in the 1960's.

In liquids, the function, F(t), of the nuclear position coordinates which contains this time dependence varies randomly as the molecules containing the magnetic nuclei undergo their Brownian motion. The value of F(t) measures the magnetic or electric coupling between the nucleus and its surroundings. The correlation function of F(t), denoted as $G(\tau)$, characterizes the differences between F(t) values over short intervals of time, τ, and is given by

$$G(\tau) = F(t)F^*(t + \tau) \tag{43}$$

The function $G(\tau)$ represents the decay in correlation as the time interval becomes larger. For the molecular processes that are of interest to us, $G(\tau)$ takes the form[31] of

$$G(\tau) = \overline{F(t)F^*(t + \tau)}e^{-\tau/\tau c} \tag{44}$$

$G(\tau)$ is an experimental time function that decays rapidly to zero when τ exceeds a particular value τ_c known as the correlation time. τ_c defines the length of the time needed by the kT randomizing force to reduce F(t) to 1/e (or 37%)

of its initial value. In NMR relaxation studies, this time constant, τ_c, is defined as the average time period in which a molecule rotates through one radian ($\approx 57^{o}$).

Symmetric-top molecules, which experience anisotropic motions, require two diffusion constants ($D_{\parallel}$ and $D_{\perp}$) to characterize the reorientational motion. If the reorienting vector is aligned parallel to the principal axis, yield a single τ_c, the correlation time is related to the rotational diffusion coefficient only and can be expressed as

$$\tau_c = 1/(6D_{\perp}) \tag{45}$$

If the reorienting vector lies at an angle θ relative to the principal axis, the correlation time will be a function of perpendicular and parallel diffusion constants. Woessner[30] has derived an equation for the correlation time as a function of θ and the two diffusion constants, $D_{\parallel}$ and $D_{\perp}$, for symmetric top molecules:

$$\tau_c = A/(6D_{\perp}) + B/(5D_{\perp} + D_{\parallel}) + C/(2D_{\perp} + 4D_{\parallel}) \tag{46}$$

where $A=0.25(3\cos^2\theta-1)^2$, $B=3\sin^2\theta\cos^2\theta$, $C=0.75\sin^4\theta$. When $\theta = 0$, the above equation will be reduced to equation (45).

For asymmetric molecules, it takes three parameters to describe the molecular rotation, and an additional parameter will be needed for the internal rotation. Since a complete

characterization of the dynamics behavior of totally asymmetric molecules in solution is very difficult,[32] most studies would assume an asymmetric molecule as a quasi-symmetric-top molecule. This simplifying assumption makes many asymmetric systems suitable for study by NMR.

CHAPTER REFERENCES

1. Bloemberg, N.; Purcell, E. M.; Pound, R. V. Phys. Rev., **1948**, 73, 679.

2. Purcell, E. M.; Torrey, H. C.; Pound, R. V. Phys. Rev., **1946**, 69, 37.

3. Bloch, F.; Hansen, W. W.; Packard, M. E. Phys. Rev., **1946**, 69, 127.

4. Abragam, A.; Principals of Nuclear Magnetism, Oxford University Press: London, **1961**.

5. Emsley, J. W.; Feeney, J.; Sutcliffe, L. H. High Resolution Nuclear Magnetic Resonance Spectroscopy, Pergamon: New York, **1965**.

6. Huntress, W. T., Jr.; J. Chem. Phys., **1968**, 48, 3524.

7. Pople, J. A.; Schneider, W. G. Bernstein, H. J. High Resolution Nuclear Magnetic Resonance, McGraw-Hill: New York, **1959**.

8. Ramsey, N. F.; Nuclear Moments, Wiley: New York, **1953**.

9. Schlichter, C. P. Principles of Magnetic Resonance, Harper and Row: New York, **1963**.

10. Tsang, T.; Farrar, T. C. J. Chem. Phys., **1969**, 50, 3498.

11. Becker, E. D. High Resolution NMR: Theory and Chemical Applications, 2nd ed.; Academic: New York, **1980**; chapter 8, p. 188.

12. Farrar, T. C.; Becker, E. D., Pulse and Fourier Transform NMR, Academic: New York, **1971**, Ch. 4.

13. Hawkes, G. E.; Elliot, J. E. J. Chem. Soc. Dalton Trans., **1984**, 279.

14. Becker, E. D.; Pulse and Fourier Transform NMR, Academic: New York, **1972**; p. 46.

15. Bender, H. J.; Zeidler, M. Ber. Bunsenges. Phys. Chem. **1971**, 75, 236.

16. Hubbard, P. S. Phys. Rev. A., **1974**, 9, 481.

17. Gleeson, J. W.; Vaughan, R. W. J. Chem. Phys., **1983**, 78, 5384.

18. Mahake, H., Spiess, H. W. J. Chem. Phys., **1974**, 61, 55.

19. Veeman, W. S. Progr. Nucl. Magn. Reson. Spectrosc., **1984**, 16, 193.

20. Fung, B. M.; Parhami, P. J. Magn. Reson., **1985**, 63, 168. and references therein.

21. Freeman, R.; Hill, H. D. W. Molecular Spectroscopy 1971, Institute of Petroleum, London, **1971**.

22. Farrar, T. C.; Druck, S. J.; Shoup, P. R.; Becker, E. D. J. Amer. Chem. Soc., **1972**, 34, 699.

23. Levy, G. C. J. Chem. Soc., Chem. Commun., **1972**, 352.

24. Levy, G. C.; Cargioli, J. D.; Anet, F. A. L. J. Amer. Chem. Soc., **1973**, 25, 1672, and earlier papers.

25. Lyeria, J. R., Jr.; Grant, D. M.; Bertrand, R. D. J. Phys. Chem., **1971**, 75, 3967.

26. Brownstein, M.; Selig, H. Inorg. Chem. **1972**, 11, 656.

27. Lyeria, J. R. Jr.; Grant, D. M. Int. Rev. Sci., Phys. Chem. Ser. **1972**, 1, 1.

28. Huntress, W. T. J. Chem. Phys., **1968**, 48(8), 3524.

29. Shimizu, H. J. Chem. Phys., **1962**, 37(4), 765.

30. Woessner, D. E. J. Chem. Phys., **1962**, 37(3), 647.

31. Bloembergen, N.; Purcell, E. M.; Pound, R. V. Nature **1947**, 160, 475.

32. Dolle, A.; Bluhm, T. Prog. NMR Spectrosc., **1989**, 21, 175.

CHAPTER III

RAMAN SPECTROSCOPY AND MOLECULAR DYNAMICS

A. Raman Spectroscopy

1. Basic Theory

The Raman effect is inelastic light-scattering of photons by atoms or molecules in nature. The incident optical photon interacts with an atom of the molecule through dipole interaction with the electronic level, which is followed by a spontaneous photon emission. In other words, this light-scattering phenomenon does not involve absorption or emission directly from the energy levels, but instead involves an intermediate virtual state. Figure 2 illustrates the energy levels and transitions of Raman and Rayleigh scattering. When it experiences an electric field, the electron cloud in a molecule is periodically perturbed and this distortion of the electron cloud results in an induced, alternating dipole moment. The polarization, $\mathbf{P}$, defined as the induced dipole moment per unit volume, is proportional to the incident electromagnetic field, $\mathbf{E}$, and can be expressed as

$$\mathbf{P} = \alpha \mathbf{E} \tag{47}$$

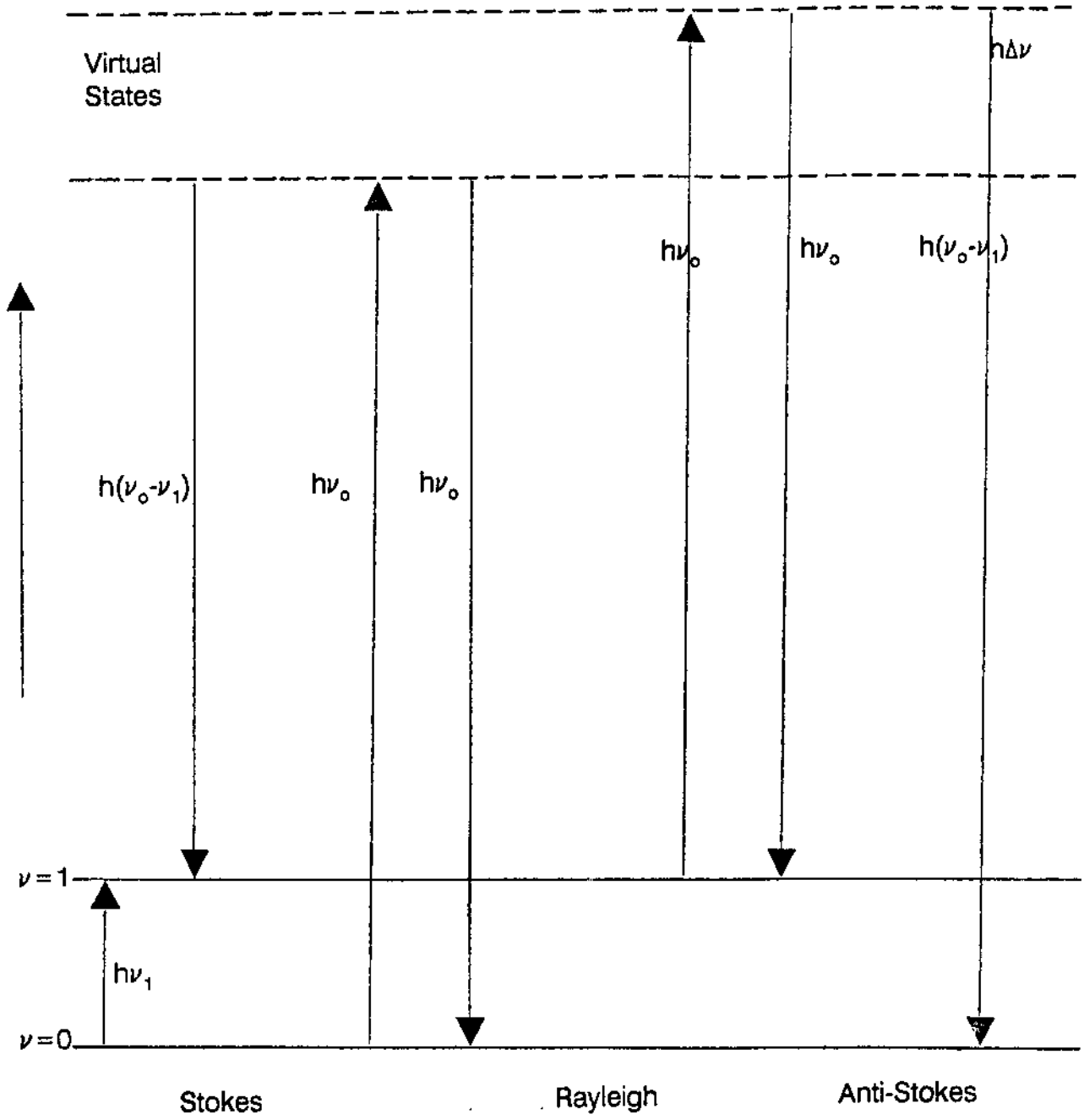

Figure 2. Energy level diagram illustrating the fundamental processes of Raman scattering. The exciting line is of energy $h\nu$. Raman bands appear at $h(\nu_o-\nu_1)$ and $h(\nu_o+\nu_1)$.

where α is the polarizability of the material. The electricfield associated with the incident beam of frequency ν_o can be written in its time-dependent form as[1]

$$E = E_o\cos(2\pi\nu_o t) \tag{48}$$

where E_o is the magnitude of the external electromagnetic wave. In this case, the polarization will fluctuate as

$$P = \alpha E_o\cos(2\pi V_o t) \tag{49}$$

The Raman effect results from the variation of the polarizability, α, at the frequency of the normal mode of the molecular vibration and α can be expressed as

$$\alpha = \alpha_o + \alpha_k\cos(2\pi\nu_k t) \tag{50}$$

The first term, α_o, represents for the static polarizability of the molecule with a fix nuclear position. The summation term expresses the polarizability changes which arise from the time-dependent normal modes of the molecule, and ν_k is the frequency of the k^{th} vibration. Introducing α, as expressed above, into equation (49), gives

$$P = \alpha_o E_o\cos(2\pi V_o t) + (E_o/2)\ \alpha_k\{\cos[2\pi(\nu_o+\nu_k)] + \cos[2\pi(\nu_o-\nu_k)]\} \tag{51}$$

The first term gives rise to the Rayleigh scattering describing a classical dipole radiating at frequency ν_o (Figure 2). The second term contains two frequency-shifted radiations at frequencies $(\nu_o + \nu_k)$ and $(\nu_o - \nu_k)$, known as anti-Stokes and Stokes Raman scattering respectively.

2. Vibrational Lineshapes and Fourier Transformations

In Raman scattering, molecular rotational and vibrational motions are known to have a certain influence on the Raman light scattering and polarizability and, thus, the frequency distribution of the scattered light contains information about the rotational motion of molecules. The life time, τ, during the re-equilibration process, leads to a line broadening or bandwidth increment, $\Delta\omega$, of the vibrational line as predicted by the energy-time uncertainty principle[2]

$$\tau\Delta E \approx \hbar \quad \text{or} \quad \tau\Delta\omega \approx 1 \tag{52}$$

As a consequence, a frequency distribution around the unperturbed vibrational frequency is exhibited and this gives rise to a band profile. The extent to which a vibrational band is broadened is governed by the relaxation process which in turn is dominated by the dynamic effects or the molecular motions. Thus, the analysis of Raman band

profiles[3] can provide us valuable information about molecular motions.

Vibrational bandshapes are a consequence of the thermal molecular motions. The spectral lines can be broadened by both molecular vibrational and rotatonal relaxation.[4,5] The relaxation process in Raman spectroscopy is the dispersion of the excess energy of the excited oscillators to molecular motion in the condensed phase. There are three types of information that can be extracted from normal vibrational spectra, namely, peak frequency, peak intensity, and lineshape. The vibrational peak maxima in the liquid phase depend on static parameters such as force constants, atomic masses, and bond distances; band profiles and bandwidths depend on dynamic parameters arising from atomic and molecular motions.

The spectral profile, $I(\omega)$, represents the frequency distribution of band intensities. In its two limits, it can assume or represent either a Gaussian or Lorentzian type distribution. The respective equations describing the two band shapes are[6]

$$I(\omega)_G = A \exp\{-\ln 2[(\omega - \omega_o)/\Delta]^2\} \tag{53}$$

and

$$I(\omega)_L = A \{ 1 + [(\omega - \omega_o)/\Delta]^2 \}^{-1} \tag{54}$$

These are both symmetrical about the peak center, ω_o. In

both equations, A is the peak intensity at the peak center, ω_o and Δ represent half of the band width at half of its maximum intensity (HWHM). It has been shown that, physically, Gaussian band shapes represent rigid molecular environments while Lorentzian profiles indicate extremely mobile environments.[6] Experimentally, very few pure Gaussian or Lorentzian profiles are encountered. Rather a combination of both is almost always the case. In the liquid phase, for small to medium size molecules, the vibrational band shape is closer to a Lorentzian type curve.[6]

The application of Raman spectroscopy to the study of dynamical processes is based on the use of a mathematical relationship known as the Wiener-Khintchine theorem.[7] Briefly, it states that for any independent dynamical variable (e.g., time), the frequency spectral profile, $I(\omega)$, of the process and the corresponding time correlation function G(t) are each other's Fourier transforms. Thus,

$$G(t) = FT[I(\omega)] \tag{55}$$

and

$$I(\omega) = FT[G(t)] \tag{56}$$

It should be noted that the relationships established in the above two equations are perfectly general with the only restriction being that a linear response should be present

between the system and the perturbing radiation. It is useful, in experiments, to sort out what frequencies are present in a complex waveform and to determine the intensity at each of these frequencies. Fourier analysis is a mathematical technique for converting a complex waveform into its spectral components.

3. Relaxation Processes

Raman vibrational line broadening in the condensed phase is due mainly to rotational and vibrational relaxation. Their contribution to the linewidth can be separated in a Raman experiment by making use of the tensor properties of the polarizability, α.[8] A Taylor series expansion of the polarizability in terms of vibrational normal coordinates allows the vibrational-rotational correlation function to be written as the product of amplitude and angle-dependent terms.[8] The time dependent development of the amplitude factor is assigned to the vibrational relaxation, whereas the time development of the angle-dependent factor is assigned to the rotational relaxation. These two types of relaxation processes are considered to be statistically independent. Vibrational and rotational types of motion are not coupled. Therefore, the overriding advantage in performing a Raman lineshape study is that it leads to the separation of the relaxation processes.

Experimentally, the deconvolution of the vibrational and rotational contributions to the band profile can be accomplished by observing the scattered light that is polarized parallel (I_{pol}) and perpendicular (I_{dep}) to the incident radiation. The observed Raman pure vibrational spectrum is given by:[9]

$$I(\omega)_{iso} = I(\omega)_{pol} - (3/4)I(\omega)_{dep} \tag{57}$$

where $I(\omega)_{iso}$ is the component of the scattered light independent of molecular orientation (isotropic). Fourier transformation of the isotropic component leads to the pure vibrational relaxation correlation function:[6]

$$FT[I(\omega)_{iso}] = FT[I(\omega)_{pol} - I(\omega)_{dep}] = G(t)_{v} \tag{58}$$

The depolarized (anisotropic) Raman spectrum contains components that are both dependent and independent on molecular orientation. Fourier transformation of the anisotropic band will result in the anisotropic correlation function $G(t)_A$:[6]

$$FT[I(\omega)_{dep}] = FT[I(\omega)_{aniso}] \tag{59}$$

and

$$G(t)_A = G(t)_V G(t)_R \tag{60}$$

Since $I(\omega)_{aniso}$ is identified with a convolution of the rotational and vibrational relaxation, it can be represented as a product of their respective time Fourier transforms. This allows a method for performing the deconvolution and obtaining the rotational correlation function, $G(t)_R$, by

$$G(t)_R = G(t)_A/G(t)_V \tag{61}$$

This vibrational-rotational separation from Raman vibrational bandshapes is only possible for totally symmetric vibrations where the pure vibrational bandshape can be obtained from the Raman spectrum.[8] The only exception occurs when the vibrational width is negligible compared to the reorientational width.[10] The determination of the predominant relaxation process is facilitated by comparing the different correlation functions at various decay values.

B. Correlation Functions

The Wiener-Khintchine theorem[7] is the foundation of the application of spectroscopic methods to studies of molecular motion. This theorem states that, for any dynamic process, the power spectrum, $I(\omega)$, of this process and the corresponding time correlation function, $f(t)$, are mutual Fourier transforms. These correlation functions can be obtained by numerical Fourier transform of experimental band

contours and can also be predicted by theoretical modeling. Thus, such correlation functions, which are strictly defined in time dependent statistical mechanics,[11-15] provide an important link with theoretical studies of molecular dynamics in the condensed phase. The small-step rotational diffusion theory[16] proposed by Debye has been extensively applied to interpret reorientational spectra from IR and Raman spectral bandwidths.

1. General Aspects

According to the fluctuation-dissipation theorem,[11,17] the energy dissipated by a system when it is exposed to an external field is related to a time-correlation function, which describes the detailed way in which spontaneous fluctuations relax the system back to the equilibrium state. Utilization of the fluctuation-dissipation theorem leads the correlation function to be expressed in a one-sided average form[6]

$$f(t) = \langle m(0)m(t) \rangle \tag{62}$$

where m(t) is defined as a tensor along the vibrational-rotational transition moment of the molecule.

In IR absorption, m(t) is identified with the first-rank dipole moment tensor (a vector), $p^{(1)}$. The dipole moment correction function, $f_p(t)$, is

$$f_p(t) = \langle p(0)p(t) \rangle \tag{63}$$

Since p(t) is fixed in the molecule frame, variations resulting from molecular motions determine the time dependence of $\langle p(0)p(t) \rangle$.

For Raman scattering, the second-rank polarizability tensor, $\alpha^{(2)}$, is involved and the polarizability correlation function is expressed as

$$f_\alpha(t) = \langle \alpha(0)\alpha(t) \rangle \tag{64}$$

The polarizability tensor ($\alpha^{(2)}$) can be separated into a product of two terms, an amplitude-dependent and an angle-dependent term,[6,18] owing to its second-rank nature. The time dependent development of the amplitude-dependent term is related to vibrational relaxation, while the angle-dependent part is dependent upon rotational relaxation.

2. Reorientational Correlation Functions

In the formalism of reorientational correlation functions, it is necessary to determine the way in which the dipole moment and polarizability change when the molecule rotates through an Eulerian angle. One general approach[2,11,18,19] is to describe the reorientation of the tensor in consideration by the rotation of the molecule frame with respect to the laboratory reference coordinate

system. This is done by expressing the Cartesian tensor elements in terms of Wigner rotation matrices.

The derived reorientational correlation functions for the dipole moment and polarizability are given as[20]

$$f_p(t) = \sum_{m=-1}^{1} |p_m^{(1)}|^2 \, g_m^{(1)}(t) \tag{65}$$

and

$$f_\beta(t) = \sum_{m=-2}^{2} |\beta_m^{(2)}|^2 \, g_m^{(2)}(t) \tag{66}$$

The coefficients in these two equations, $|P_m^{(1)}|$ and $|\beta_m^{(2)}|$ are spherical components of dipole moment and polarizability derivative respectively. They are related to the Cartesian components in the molecular frame by[11,19,21]

$$\begin{aligned} P_o^{(1)} &= P_z \\ P_\pm^{(1)} &= \mp 2^{-1/2}(P_x \pm iP_y) \end{aligned} \tag{67}$$

and

$$\begin{aligned} \beta_o^{(2)} &= (3/2)^{1/2}\beta_{zz} \\ \beta_\pm^{(2)} &= \beta_{zx} \mp i\beta_{zz} \\ \beta_\pm^{(2)} &= -(1/2)(\beta_{xx} - \beta_{yy}) \end{aligned} \tag{68}$$

Based on the small-step rotational diffusion theory,[16] the reorientational correlation functions for IR absorption and Raman scattering, $g_m^{(1)}$ and $g_m^{(2)}$, are exponential functions, $g_m^{(1)}(t) = \exp(-t/\tau_m^{(1)})$. The form of the corelation function is completely specified by the

correlation time, $\tau_m^{(1)}$, and the following results are obtained

$$f_p(t) = \sum_{m=-1}^{1} |p_m^{(1)}|^2 \exp(-t/\tau_m^{(1)}) \quad (69)$$

and

$$f_\beta(t) = \sum_{m=-2}^{2} |\beta_m^{(2)}|^2 \exp(-t/\tau_m^{(2)}) \quad (70)$$

For symmetric-top molecules, the correlation time, $\tau_m^{(1)}$, is related to rotational diffusion constants by[11,22]

$$1/\tau_m^{(1)} = l(l+1)D_\perp + m^2(D_\parallel - D_\perp) \quad (71)$$

where $l = 1$ for IR and $l = 2$ for Raman.

3. Correlation Functions and Symmetry of Molecules

For molecules of C_{3v} or higher symmetry, the relationship between spherical components can be expressed as

$$|p_m^{(1)}| = |p_{-m}^{(1)}| \quad (72)$$

and

$$|\beta_m^{(2)}| = |\beta_{-m}^{(2)}| \quad (73)$$

Therefore, simplified forms of equations (69) and (70) can be written as follow:

$$f_p^{(1)} = |p_0^{(1)}|^2 \exp(-t/\tau_0^{(1)})$$

$$+ 2|p_1^{(1)}|^2\exp(-t/\tau_1^{(1)}) \qquad (74)$$

and

$$f_\beta^{(1)} = |\beta_0^{(2)}|^2\exp(-t/\tau_0^{(2)}) + 2|\beta_1^{(2)}|^2\exp(-t/\tau_1^{(2)}) + 2|\beta_2^{(2)}|^2\exp(-t/\tau_2^{(2)}) \qquad (75)$$

The above two expressions reveal the fact that a reorientational IR or Raman correlation function of a band contour is a linear combination of two or three time-independent function terms with coefficients being the squares of the spherical IR or Raman tensor component in the molecular coordinate system. In general, one or more terms vanish due to symmetry properties.

By reference to the character table, the number of non-vanishing terms for a vibrational mode can be determined from the point group of the molecule in consideration via the transformation properties of these spherical components in equations (67) and (68).

For E" vibrational modes of D_{3h} molecules, it is found that

$$\beta_o^{(2)} = (3/2)^{1/2}\beta_{zz} = 0 \qquad (76)$$

and

$$\beta_2^{(2)} = -(1/2)(\beta_{xx}-\beta_{yy})+i\beta_{xy} = 0 \qquad (77)$$

Therefore, the total reorientational correlation function becomes a single exponential term.

For E vibrational modes in C_{3v} molecules,

$$\beta_o^{(2)} = (3/2)^{1/2}\beta_{zz} = 0 \tag{78}$$

and the total reorientational correlation function becomes a sum of two exponential functions.

$$f_{Raman}^{E}(t) = 2|\beta_1^{(2)}|^2\exp(-t/\tau_1^{(2)}) + 2|\beta_2^{(2)}|^2\exp(-t/\tau_2^{(2)})\} \tag{79}$$

4. Lorentzian Bandshapes

The small-step rotational diffusion theory proposed by Debye has been extensively applied to interpret reorientational spectra from IR and Raman studies of various molecules in condensed phases.[9] The major conclusion from this theory is that the reorientational correlation function is an exponential function, $f_m^{(l)}(t) = \exp(-t/\tau_m^{(l)})$. The form of the correlation function is completely specified by the correlation time, $\tau_m^{(l)}$. The correlation function can be obtained simply as the inverse of the half width at half maximum intensity (HWHM), Δ', since an inverse Fourier transform of the exponential function gives a Lorentzian bandshape in the frequency domain, $I_{Lor}(\omega) = A/[1 + (\omega/\Delta)^2]$, as shown in the following.

$$I(\omega) = (1/2\pi)\int \exp(-t/\tau_m^{(1)})\exp(i\omega t)dt$$

$$= (A\Delta'\pi/2\pi)\int \exp(-\Delta'|t|)\exp(-i\Delta' t)dt$$

$$= (A\Delta'/2)[\int \exp[t(\Delta'-iw)]dt + \int \exp[t(-\Delta'-iw)]dt]$$

$$= (A\Delta'/2)[1/(\Delta'-i\omega) + 1/(\Delta'+i\omega)] = A\Delta'^2/(\Delta'^2 + \omega^2)$$

$$= A/[1 + (\omega/\Delta')^2] \qquad (80)$$

where $\Delta' = 1/(\pi c\tau)$.

The lineshape of the E" vibration of D_{3h} molecules is a single Lorentzian, whereas the inverse Fourier transform of equation (79) gives a sum of two Lorentzians for the E vibrations of C_{3v} molecules. Therefore, the experimental evaluation of the band contour of a doubly degenerate vibrational-rotational Raman E mode yields a reorientational correlation function that mixes indices m = 1 and m = 2.

5. Bandwidth Increments and Rotational Relaxation

The bandwidth, Δ, employed in our research is the full width at half maximum intensity (FWHM) in wavenumber (cm^{-1}). Thus a conversion factor, πc, is necessary to relate the bandwidth, Δ, and the correlation time, τ, by

$$\Delta = (\pi c\tau)^{-1} \qquad (81)$$

Through the correlation function formalism, the bandwidth increment resulting from the rotational relaxation, Δ_{rot}, is related to rotational diffusion constants by the expression

$$\Delta_m^{(1)}(\text{rot}) = (\pi c \tau_m^{(1)})^{-1}$$
$$= (\pi c)^{-1}[1(1 + 1) + m^2(D_{\parallel} - D_{\perp})] \quad (82)$$

C. Raman Experiment

1. The Raman Spectrometer and Spectrum Recording

The schematic diagram of the Laser Raman spectrometer is illustrated in Figure 3. The irradiation source is an argon ion laser radiating at 4880 Å. The laser beam was focused into the sample and the scattered light was collected through a polarization analyzer and polarization scrambler into the entrance of a Spex 14018 scanning double monochromator. The sample was contained in a sealed melting point capillary tube, which was inserted into a Harney-Miller cell. Temperature regulation, if needed, was accomplished via liquid nitrogen boil-off or heated air flow, and measured with an iron-constantan thermocouple positioned adjacent to the sample. Both polarized and depolarized spectra were acquired at 90° to the incident laser beam. Detection was accomplished using a cooled (to -30°C) RCA-C31034 photomultiplier and photon counting electronics.

Slit widths (SW), depending on the spectral intensities, were set to gain resolution for various vibration modes. Frequency increments ($\Delta\omega$) were chosen to satisfy the condition for the convolution procedure, which is a computational process employed to eliminate

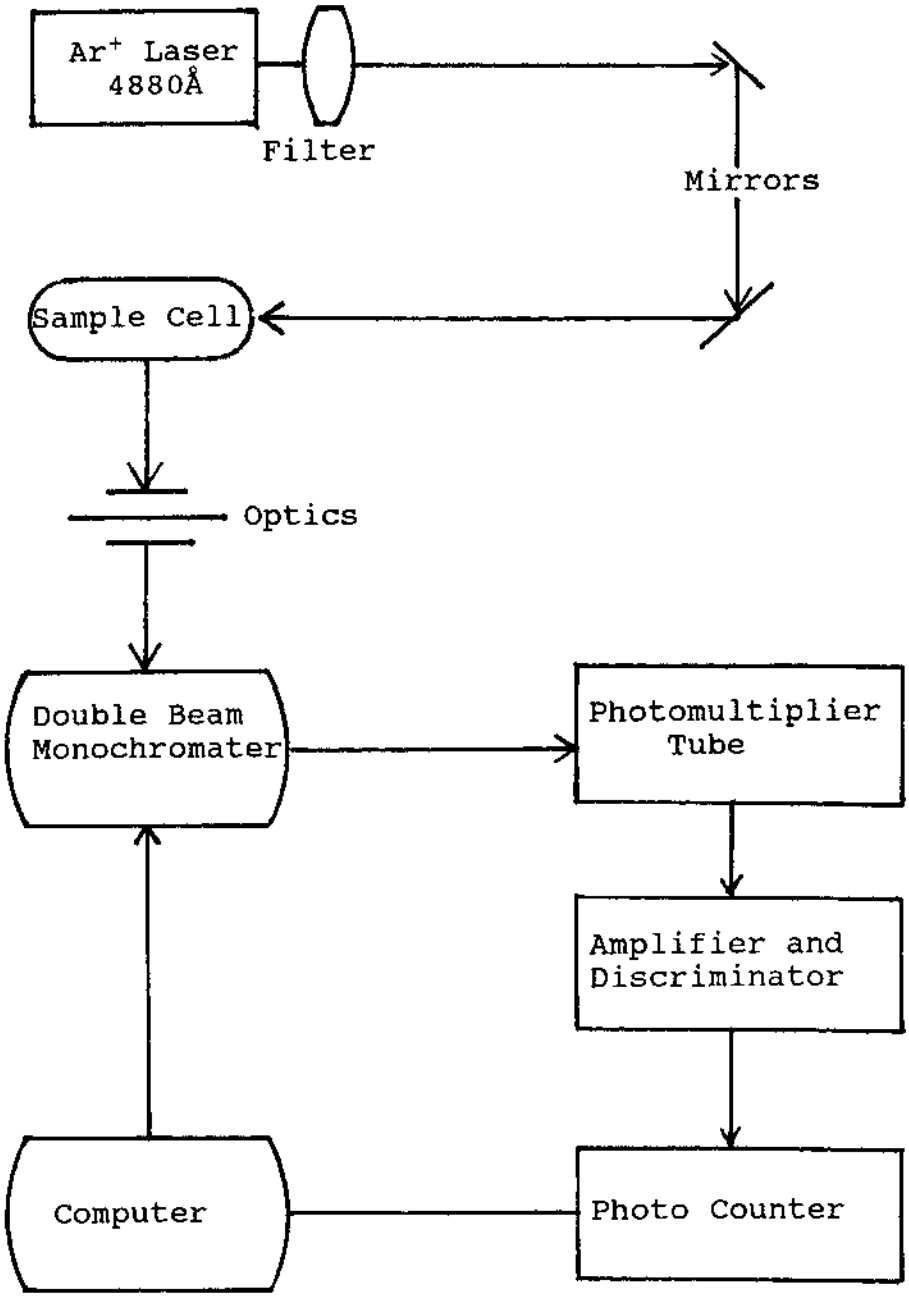

Figure 3 Schematic diagram of the laser Raman spectrometer

instrumental influences on spectral linewidths. The resultant signals, intensities in photon counts per second (CPS), were recorded digitally through an interfaced microprocessor and stored on floppy diskettes for further processing.

2. Raman VV and VH Experiments

Experimentally, separation of vibrational and rotational relaxations is achieved by the VV-VH Raman experiment. Interacting with polarized incident light, a non-spherical molecule can scatter both polarized and depolarized radiation.

In the Raman VV experiment, polarized light is observed, whereas the depolarized radiation can be recorded through VH experiments. The isotropic spectrum, which is independent of rotational relaxation, can be determined from a combination of VV and VH experiments by the standard relationship,

$$I_{iso}(\omega) = I_{pol}(\omega) - (4/3)I_{dep}(\omega) \qquad (57)$$

A scheme of polarized light scattering is shown in Figure 4. The scattered light is observed at right angles to the laser radiation polarized in the XZ-plane, demonstrated by vertical arrows. Polarized (vertical arrows in the XZ-plane) and depolarized (horizontal arrows in the XY-plane) radiations can be detected separately by orienting

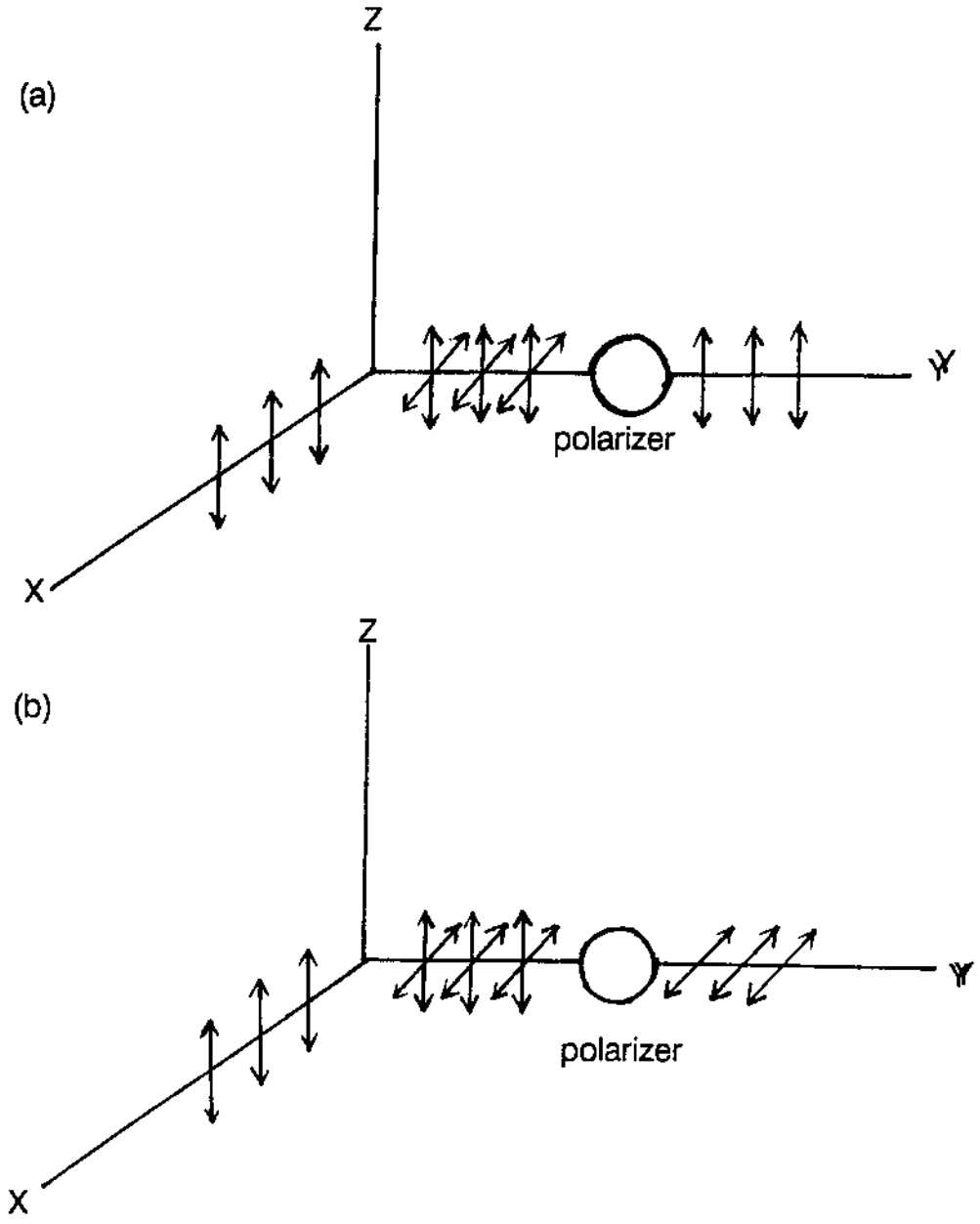

Figure 4. Polarized and depolarized spectra recording. (a) Parallel-oriented polarizer transmits polarized radiation (YZ plane) only. (b) Perpendicular-oriented polarizer transmits depolarized radiation (XY plane) only.

a polarizer properly. In the VV experiment, Figure 4 (a), the polarizer is parallel-oriented and permits passage of the polarized radiation only. The polarizer is rotated through 90° in the VH experiment onto the XY-plane, as shown by Figure 4 (b). This perpendicular arrangement blocks the polarized radiation and only the depolarized radiation enters the spectrometer slit.

3. Bandshape Analysis and Curve-fitting

Ever since the pioneering work of molecular dynamics studies by Gordon[23], analysis of Raman and/or IR bandshapes to quantitatively determine dynamic properties of molecules has become a rapidly expanding field of study. As described by equation (52), an equivalent relationship between bandwidth increment and relaxation time, it can also be expressed as $\tau = (\Delta\omega)^{-1}$. A fast motion results in a fast relaxation (a short τ) and, consequently, a large bandwidth increment is exhibited in the spectral band profile.

One major barricade to bandshape analysis is the overlap of band contours of different vibrational modes due to a high extent of line broadening. Fundamental vibrational bands may overlap, through Fermi resonance, with overtones or combinational bands arising from vibrational anharmonicity, usually present their use in bandshape studies. As the size of molecule gets bigger and symmetry becomes lower, the overlapping becoming worse. The band overlap due to line broadening also can result from various

factors including hot bands, isotope splitting, poor resolution, low intensity, etc., which makes analyses difficult.

Bandwidth obtained by hand measurement is possible when there is no overlap problem occur. However, in order to obtain true bandwidths from the bandshape interfering with the factors mentioned above, these problems must be solved by curve-fitting procedures with proper models based on the theoretical and/or available experimental data to disentangle these band contours. The complete procedure includes baseline subtraction, bandwidth computation, as well as slitwidth correction.

a. Baseline Correction

The baseline correction of the recorded spectrum was performed by two-frequency baseline subtraction. Assuming a linear function of the frequency, i.e., $I_{BL}(\omega) = a + b\omega$, the baseline was calculated from the two frequencies selected from each side of the peak contour. The coefficients, a and b, were determined by least-square fit to seven points about each selected frequency. The baseline subtracted spectrum $I_{BS}(\omega)$, is obtained by

$$I_{BS}(\omega) = I_{exp}(\omega) - (a + b\omega) \tag{83}$$

b. Slitwidth Correction

The observed spectrum, I_{exp}, is a convolution of the true spectrum, $I_{true}(\omega)$, and the instrumental slit function, $S(\omega)$, given as

$$I_{exp}(\omega) = \int_{-\infty}^{\infty} I_{true}(\omega') S(\omega - \omega') d\omega' \qquad (84)$$

where ω and ω' are the frequency displacements from the laser line. The instrumental slit functions were measured by passing the laser line through the monochromater at various slit settings. Filters, with attenuations of 10^2 to 10^5, were used to avoid damage to the photomultiplier tube. The convolution procedure is to find $I_{true}(\omega)$ from a knowledge of $S(\omega)$ and $I_{exp}(\omega)$ by best fitting to equation (84).

The recorded signal from each measurement was well represented by a triangle-shape peak. The full width at half maximum of this peak was measured as the instrumental slitwidth (SW). Assuming a normalized triangular slit function, a 19-point convolution was employed. Figure 5 illustrates the methodology of this experimental procedure. At each point, $10 \geq i \geq 1$, the function value is thus given by

$$G(i) = SW^{-1}[1 - (10 - i)\Delta\omega/SW] \qquad (85)$$

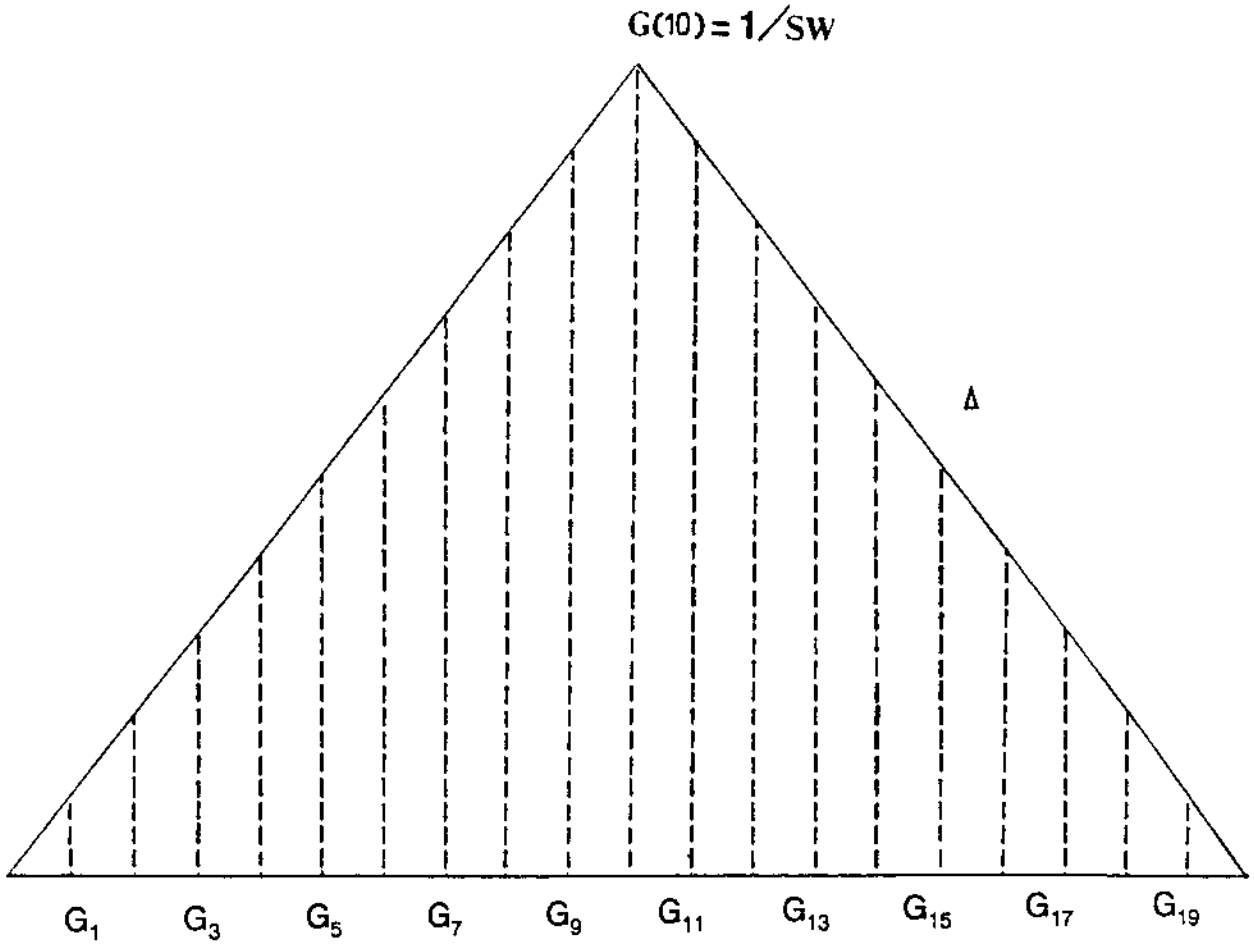

$$G(1) = G(19) = (1/SW)(1 - 9\Delta/SW)$$
$$G(2) = G(18) = (1/SW)(1 - 8\Delta/SW)$$
$$\vdots$$
$$G(8) = G(12) = (1/SW)(1 - 2\Delta/SW)$$
$$G(9) = G(11) = (1/SW)(1 - \Delta/SW)$$

Figure 5. 19-point slit convolution.
Δ stands for experimental frequency increment
SW is instrumental slit width

where $\Delta\omega$ is the frequency increment and G(i) = 0 if $(10 - i)\Delta\omega \geq SW$. For $i \geq 10$, G(i) = G(20 - i). Then the integral is performed via the Simpson's rule.[24]

c. Bandwidth Computation

The experimental intensities were fitted with theoretical Lorentzian lineshapes. The fitting was done computationally by using non-linear regression to minimize root-mean-square errors between experimental and computed data. The elimination of the effects of instrumental linebroadening was performed by convolution of the calculated spectra with a 19-point triangular slit function. The frequency increment setup in data acquisition was limited by the condition, $(\Delta\omega) \geq SW$. Computed bandwidths used to determine reorientational diffusion constants were full width at half maximum (FWHM) intensity.

D. Determination of Rotational Diffusion Constants By Raman Lineshape Analysis of C_{3v} Molecules

The reorientational experimental bandwidth increment, Δ_{exp}, has been proven by Gordon[25], Bartoli, and Litoritz,[4] to arise from the combination of vibrational relaxation, Δ_{vib}, and rotational relaxation, Δ_{rot}

$$\Delta_{exp} = \Delta_{vib} + \Delta_{rot} \tag{86}$$

Therefore, it is necessary to convert vibrational band widths before diffusion constants can be obtained. This

correction can be performed experimentally by using the isotropic Raman spectrum[4,5,26] of totally symmetric vibrations. This feat comes from the tensor property of the polarizability, α. A Taylor series expansion of this second-rank tensor allows the vibrational-rotational correlation function to be expressed as the product of an amplitude-dependent and an angle-dependent factor.[6,20] The time dependent development of the amplitude-dependent factor is assigned to vibration relaxation, whereas the angle-dependent factor is assigned to rotational relaxation.

1. A_1 Modes

a. Determination of Δ_{vib}

In Raman spectroscopy, one can obtain both polarized (I_{pol}) and depolarized (I_{dep}) linewidths. The observed Raman pure vibrational isotropic spectrum can be obtained by[6,27]

$$I(\omega)_{iso} = I(\omega)_{pol} - (4/3)I(\omega)_{dep} \qquad (57)$$

where $I(\omega)_{iso}$ is the component of the scattered intensity resulting only from vibrational relaxation (i.e., independent of molecular orientation). Therefore, isotropic linewidths are equal to vibrational relaxation linewidths

$$\Delta_{iso} = \Delta_{vib} \qquad (87)$$

b. Separation of Δ_{vib} and Δ_{rot}

The depolarized (i.e., anisotropic) Raman spectrum contains both vibrational and reorientational components (i.e., dependent on both vibrational and rotational motions). The linewidth term can be expressed as

$$\Delta_{aniso} = \Delta_{dep} = \Delta_{vib} + \Delta_{rot} \tag{88}$$

The combination of equations (89) and (90) leads to the expression of the bandwidth increment resulting from rotational relaxation,

$$\Delta_{rot} = \Delta_{aniso} - \Delta_{iso} \tag{89}$$

c. Evaluation of the Tumbling Diffusion Constant

The analysis of isotropic and anisotropic linewidths of totally symmetric vibrations is a well established, reliable technique to determine the tumbling diffusion constants of symmetric-top molecules.[5,6,9,19] By using the small-step rotational diffusional model,[16,19,22] the bandwidth Δ_{rot} is related to rotational diffusion constants by

$$\Delta_{rot} = (1/\pi c)[J(J + 1)D_{\perp} + m^2(D_{\parallel} - D_{\perp})] \tag{82}$$

where n is the rank of the tensor involved in the description of each spectroscopic process, m is an integer

depending on the symmetry of the individual vibrational modes, which can be 0, ±1, or ±2. For totally symmetric Raman A_1 modes in C_{3v} molecules, I=2, and m=0, thus eq. (82) can be reduced to

$$\Delta_{rot} = 6D_{\perp}/\pi c \tag{90}$$

and the anisotropic linewidth is expressed as

$$\Delta_{aniso} = \Delta_{vib} + 6D_{\perp}/\pi c \tag{91}$$

By introducing eq. (89) into eq. (90), one may obtain

$$D_{\perp} = (\Delta_{aniso} - \Delta_{iso})\pi c/6 \tag{92}$$

2. E Modes

The Raman lineshape of E vibrations is a sum of two Lorentzian bands with the same peak center and relative bandwidths, $\Delta_1^{(2)} < \Delta_2^{(2)}$ (if $D_{\parallel} > D_{\perp}$). These bandwidths are related to rotational diffusion constants as

$$\Delta_1^{(2)} = \Delta_{vib} + (5D_{\perp} + D_{\parallel})/\pi c \tag{93}$$

and

$$\Delta_2^{(2)} = \Delta_{vib} + (2D_{\perp} + 4D_{\parallel})/\pi c \tag{94}$$

In order to calculate the spinning diffusion constants,

$\Delta_{vib}(A_1)$ obtained from the linewidth of the isotropic band profile must be used to eliminate $\Delta_{vib}(E)$ since there is no isotropic scattering from E vibrations. This is done by using the proportionality, $\Delta_{vib} \propto (1/\Delta)^2$, predicted by the Fisher-Laubereau IBC model[27] via the expression

$$\Delta_{vib}(E) = \Delta_{vib}(A_1)[\omega(A_1)/\omega(E)]^2 \qquad (95)$$

In the above expression, $\Delta_{vib}(A_1)$ is the isotropic width of an A_1 mode involving the same motion as the E vibration, and the second term on the right is the squared ratio of their frequencies.

As found in many systems,[28,29,30] $\Delta_2^{(2)}$ is often found to be broader than may be explained solely upon the basis of molecular reorientation and vibration; it has been suggested that the additional width may result from collision-induced scattering in the wings of the spectrum.[28,31] Using the narrower component, $\Delta_1^{(2)}$, of E modes to calculate $D_\parallel$ is the key point of the approach. With $D_\perp$ obtained from Raman A_1 modes and $\Delta_v(E)$ from the corresponding $\Delta_v(A_1)$, one can derive $D_\parallel$ from the following expression

$$D_\parallel = (\Delta_1^{(2)} - \Delta_{vib})\pi c - 5D_\perp \qquad (96)$$

CHAPTER REFERENCES

1. Tobin, M. C. Laser Raman Spectroscopy; Wiley, New York, **1971**, p. 6.

2. Messiah, A. Quantum Mechanics I, Wiley: New York, **1958**, p.p. 135-138.

3. The Raman bandwidths are computed by fitting the band profiles using a computer program, written in Fortran code, obtained from QCPE, Department of Chemistry, Indiana University, Bloomington, Indiana 47405.

4. Bartoli, F. J.; Litovitz, T. A. J. Chem. Phys., **1972**, 56, 413.

5. Bratos, S.; Marechal, E. Phys. Rev., **1971**, A4, 1078.

6. Rothschild, W. G. Dynamics of Molecular Liquids, Wiley-Interscience, New York, **1984**.

7. Wang, M. C.; Uhlenbeck, G. E. Rev. Mod. Phys., **1945**, 17, 323.

8. Wilson, E. B.; J. C. Decius; P. C. Cross, Molecular Vibrations, McGraw-Hill, New York, **1955**.

9. Clarke, R. J. H.; Hester, R. E. Advances in Infrared and Raman Spectroscopy; Hyden: London, **1978**.

10. Marsult, J. P.; Marsault-Herial, F.; Levi, G. J. Chem. Phys., **1975**, 62, 893.

11. Berne, B. J.; Harp, G. D. Adv. Chem. Phys., **1970**, 17, 63.

12. Berne, B. J. Physical Chemistry: An Advanced Treatiese; Eyring H., Henderson D., Jost, W. ed.; Academic: New York, **1970**, Vol. VIII B, p. 539.

13. Kubo, R. Lectures in Theoretical Physics; Vol. 1, Interscience, New York, **1961**, p. 120.

14. Zwanzig, R. Ann. Rev. Phys. Chem., **1965**, 16, 67.

15. Forster, D. Hydrodynamic Fluctuation, Broken Symmetry and Correlation Functions; Benjamin, **1975**.

16. Debye, P. Polar Molecules, Dover, New York, **1928**.

17. (a) Kubo, R. J. Phys. Soc. Jap., **1975**, 12, 570. (b) Kubo, R. Rep. Prog. Phys., **1966**, 29 (Part 1), 255.

18. Reuven, A. B.; Gershon, N. D. J. Chem. Phys., **1969**, 51, 893.

19. Steele, W. A. Transport Phenomena in Fluids; Hanley H. J. M. ed., Marcel Dekker: New York, **1969**, Chapter 8.

20. Clarke, R. J. H. In Advances in Infrared and Raman Spectroscopy; Hester, R. E. and Clarke, J. H. R., Eds.; Hyden: London, Vol. 4, **1978**; p 109.

21. Rose, M. E. Elementary Theory of Angular Momentum; Wiley: New York, **1957**.

22. Valiev, K. A. Opt. Spektrosk., **1962**, 13, 282.

23. (a) Gordon, R. G. J. Chem. Phys., **1963**, 39, 2788. (b) Gordon, R. G. J. Chem. Phys., **1965**, 42, 3658.

24. Margenau, H.; Murphy, G. M. The Mathematics of Physics and Chemistry; Second Edition, Nostrand: Toronto, **1968**, p. 477.

25. Gordon, R. G. J. Chem. Phys., **1964**, 40, 1973.

26. (a) Nafie, L. A.; Fanconi, B. Penticolas, W. L. J. Chem. Phys., **1970**, 52, 1584. (b) Nafie, L. A.; Fanconi, B. Penticolas, W. L. J. Chem. Phys., **1972**, 57, 3145.

27. Fischer, S. F.; Laubereau, A. Chem. Phys. Lett., **1975**, 35, 6.

28. Gormpf, J.; Versmold, H.; Langer, H. Ber. Bunsenges. Phys. Chem. **1982**, 86, 1114.

29. Wang, S. P.; Yuan, P.; Schwartz, M. J. Raman Spectrosc. **1989**, 20, 339.

30. Wang, S. P.; Hu, W. P.; Schwartz, M. Molecular Phys. **1989**, 68, 1125.

31. Bucao, T. A.; Litovitz, T. A. J. Chem. Phys. **1971**, 54, 3846.

CHAPTER IV

A STUDY of ^{13}C SPIN-LATTICE RELAXATION TIMES OF 2-SUBSTITUTED PENTACYCLO[6.3.0.0^{2,6}.0^{3,10}.0^{5,9}]UNDECANES IN SOLUTION

A. Introduction

The study of NMR relaxation is a well established method extensively used to study and characterize the reorientational dynamics behavior of molecules in solution[1] and in the liquid phase. Due to the difficulties[2] in characterizing completely asymmetric molecules, most studies have been confined to spherical top molecules, for which the rotation is the same about all three axes, and small symmetric top[1] molecules, for which the rotation about two of the axes are equivalent.

The goal of this investigation is to extend molecular diffusional characterization to larger molecules, since larger molecules usually lack sufficient symmetry. The polycyclic "cage" system,[3] 2-substituted pentacyclo [6.3.0.0^{2,6}.0^{3,10}.0^{5,9}]undecanes (Trishomocubanes, THCs), was targeted as substrates for this NMR relaxation study. THC is a relative large cyclic molecule and has a D_{3h} symmetry. Four 2-substituted trishomocubanes were synthesized with derivatives as shown in Figure 6.

These substituted D_3-trishomocubanes (THCs) are

relatively large (C_{11}) rigid polycyclic molecules, in which the substitutents are attached to one of the two carbon atoms [C(2) and C(9)] that lie on the threefold molecular symmetry axis. An assumption that the substituted trishomocubanes are pseudo-symmetric top molecules, whose principal axes coincide with the C_3 axis of the parent molecule, is necessary in order to proceed with the analysis. In order to determine the effects of temperature and intermolecular interactions on the reorientational dynamics in this series of THC derivatives, ^{13}C NMR relaxation times and nuclear Overhauser enhancement (NOE) have been measured as a function of temperature in the solvent chloroform for THC and its derivatives.

B. Experiments

1. Synthesis of THC Compounds

The synthesis of these trishomocubanes was performed by the post-doctoral associates in Dr. Alan P. Marchand's research group.

2. X-ray Crystal Structure of THC compounds

The X-ray crystallographic studies were performed by Dr. William H. Watson and his group at Texas Christian University. The structure of pentacyclo-[6.3.0.$0^{2,6}$.$0^{3,10}$.$0^{5,9}$]undecane-2-carboxylic acid (**1b**) was solved by direct methods and refined by using least-squares

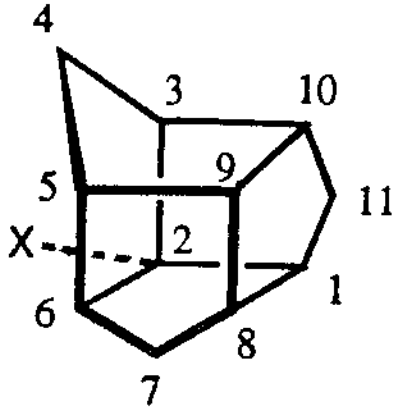

$\alpha = C(2)$

$\beta = C(1), C(3), C(6)$

$\gamma(CH_2) = C(4), C(7), C(11)$

$\gamma(CH) = C(5), C(8), C(10)$

$\delta = C(9)$

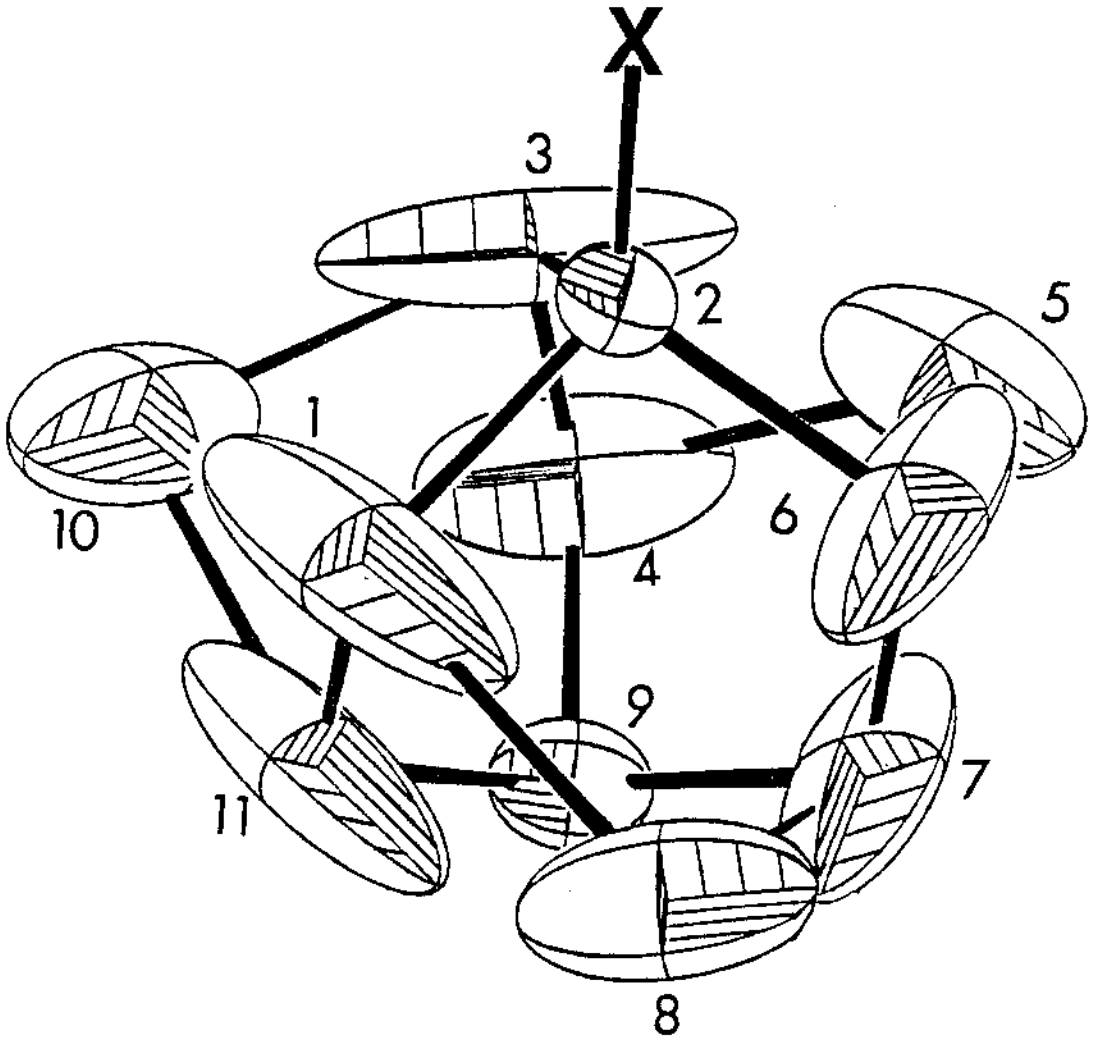

Figure 6. Structures of Trishomocubane (THC) Compound and Its Derivatives. **1a**: X=H; **1b**: X=CO_2H; **1c**: X=CO_2Me; **1d**: X=CH_2OH; **1e**: X=$C(O)NH_2$.

procedure. Due to crystal packing effects and also hydrogen bonding of the carboxyl group, the molecule experiences a large thermal oscillation around the C(2)-CO_2H axis. Due to the small number of observed data, the structure was not refined below 18%.

3. NMR Spin-Lattice Relaxation Experiment

a. NMR Sample Preparation

The THC samples for this ^{13}C spin-lattice relaxation study were prepared gravimetrically[4] and placed in 5mm NMR tubes. The solutions were degassed by applying three freeze-pump-thaw cycles. After the procedure had been completed, the NMR tubes were flame sealed in vacuo.

b. ^{13}C Spin-Lattice Relaxation Measurements

^{13}C NMR experiments were performed as a function of temperature at B_o = 4.70 T (ν_o = 50.29 MHz) using a Varian Gemini-200 FT NMR spectrometer. Spin-lattice relaxation times (T_1) and nuclear Overhauser enhancement (NOE) of the β [C_1, C_3, and C_6], $\gamma(CH_2)$ [C_4, C_7, and C_{11}], γ(CH) methinyl [C_5, C_8, and C_{10}], δ [C_9] and α [C_2 in 1a] carbons were measured three times at each temperature. The α and δ carbons are equivalent in the parent hydrocarbon, 1a.

T_1 data were acquired by using the inversion recovery pulse sequence,[5] $(180^o\text{-}\tau\text{-}90^o\text{-}A_t\text{-}D)_n$, with ten τ-values which ranged from 0.1 to 1.5 times of the estimated T_1, plus a

final value for $\tau \to \infty$. Spin-Lattice relaxation times, T_1, were determined via a nonlinear three parameters (M_o, $\cos\theta$, T_1) regression by using the magnetization equation,[6]

$$M(\tau) = M_o\ [1-(1-\cos\theta)e^{-t/T1}] \qquad (97)$$

NOE values were measured by using standard gated decoupling methods.[7] Carbon-13 chemical shifts were measured in ppm downfield from internal tetramethylsilane (TMS).

c. Data Analysis

The average observed relaxation times at each temperature were fitted by using the semi-logarithmic Arrhenius equation in order to minimize the propagation of random errors and the interpolated values of T_1 for **1a** (Table I) were used subsequently in all further calculations. The NOE values which appear in the 5th column of Table I represent the interpolated values obtained from a linear fit to the original data. The relaxation times and NOE data obtained for compounds **1b-1e** are given in Tables II through Table V.

The contribution of C-H dipolar interactions to the ^{13}C relaxation time may be obtained from the experimental T_1 and NOE using the relation, $T_{1DD} = (\frac{1}{2}\gamma_H/\gamma_C)\cdot T_1/(NOE-1) = 1.988\cdot T_1/(NOE-1)$,[8] where γ_H and γ_C are the ^1H and ^{13}C magnetogyric ratios, respectively. The results obtained for

1a are displayed in the penultimate column of Table I. T_{1DD}, in turn, is dependent upon the rotational correlation time, τ_c, of the C-H vector, which is approximately the time for the vector to reorient by one radian. The relationship between T_{1DD} and τ_c is given by $T^{-1}_{1DD} = n_H\gamma_H^2\gamma_C^2\hbar^2\tau_c/r_{CH}^6$,[9] where n_H is the number of directly bonded protons, $\hbar=h/(2\pi)$, and r_{CH} is the C-H bond length. Correlation times for the various carbons in **1a** are given in the last column of Table I. Rotational correlation times, τ_c, have been measured for three independent vectors in **1a** and also in **1b-1e**. Nonlinear regression methods which minimized the sum of the squared error between experimental and calculated rotational correlation times ($[\tau_{c,i}(exp)-\tau_{c,i}(cal)]^2$) were used to determine $D_\perp$ and $D_\parallel$ values at each temperature. Alternatively, τ_c data obtained at all temperatures were fit simultaneously by Arrhenius expressions, $D_\perp=(D_\perp)_o e^{-E_\perp/RT}$ and $D_\parallel=(D_\parallel)_o e^{-E_\parallel/RT}$. The results thereby obtained were found to be virtually identical to those generated from individual data fits at each temperature.

4. Molecular Modeling

Extraction of diffusional coefficients from $T_{1,DD}$ data requires knowledge of the structural geometry of the reorienting species (i.e., bond lengths and angles). A theoretical basis for extracting rotational diffusion coefficients from NMR relaxation time data has been

developed by Woessner.[10] The dipole-dipole relaxation times ($T_{1,DD}$) calculated from these parameters have been analyzed by the application of Woessner's equations, assuming the THC reorient as axially symmetric ellipsoids. The angle, θ, is necessary for the determination of τ_c by the application of Woessner's equation,

$$\tau_c = A/(6D_\perp) + B/(5D_\perp + D_\parallel) + C/(2D_\perp + 4D_\parallel) \qquad (46)$$

where $A=0.25(3\cos^2\theta-1)^2$, $B=3\sin^2\theta\cos^2\theta$, $C=0.75\sin^4\theta$.
A molecular modeling program,[11] MOBY, was utilized to construct the carbon skeleton of THC from the reported crystallographic data on 4,10-ethylene dioxypentacyclo [6.3.0.$0^{2,6}$.$0^{3,10}$.$0^{5,9}$]undecane-4-oxyacetic acid[12] and the angles, θ's, for each C-H vector were obtained from this structure. Protons were added to the structure and C-H bond lengths and angles were optimized via a quantum mechanical energy minimization that utilized the semi-empirical AM1 method.[13] Values of θ were also determined via classical molecular mechanics[14] geometry optimization procedures. The results agreed closely with those obtained via the corresponding quantum mechanical calculation.

C. The Results of NMR Studies

The experimental ^{13}C T_1 values, NOE's, and the correlation times for various carbon atoms in **1a-1e** as a

Table I. ^{13}C NMR Relaxation and Correlation Times in Trishomocubane

T (°C)	Carbon[a]	θ	T_1[b]	NOE	T_{1DD}[b]	τ_c[c]
46	α,δ	0	18.40	2.83	19.99	2.33
	β,γ(CH)	53°,127°	18.12	2.73	20.82	2.12
	$\gamma(CH_2)$	47.3°,132.7°	10.14	2.99	10.14	2.29
34	α,δ	0	16.38	2.86	17.51	2.66
	β,γ(CH)	53°,127°	17.23	2.76	19.51	2.43
	$\gamma(CH_2)$	47.3°,132.7°	9.12	2.99	9.12	2.55
22	α,δ	0	14.13	2.88	14.94	3.12
	β,γ(CH)	53°,127°	14.51	2.79	16.12	2.89
	$\gamma(CH_2)$	47.3°,132.7°	7.94	2.99	7.94	2.93
10	α,δ	0	12.60	2.91	13.11	3.55
	β,γ(CH)	53°,127°	12.99	2.82	14.19	3.28
	$\gamma(CH_2)$	47.3°,132.7°	7.13	2.99	7.13	3.27
-5	α,δ	0	10.44	2.94	10.70	4.35
	β,γ(CH)	53°,127°	10.82	2.87	11.50	4.05
	$\gamma(CH_2)$	47.3°,132.7°	5.97	2.99	5.97	3.90
-22	α,δ	0	8.21	2.97	8.29	5.62
	β,γ(CH)	53°,127°	8.56	2.93	8.82	5.28
	$\gamma(CH_2)$	47.3°,132.7°	4.77	2.99	4.77	4.88
-42	α,δ	0	5.92	2.99	5.92	7.87
	β,γ(CH)	53°,127°	6.22	2.99	6.22	7.49
	$\gamma(CH_2)$	47.3°,132.7°	3.50	2.99	3.50	6.65

a) α,δ represents the apical carbons (C_2,C_9) [41.5 ppm]
β represents the methinyl carbons (C_1,C_3,C_6) [47.6 ppm]
$\gamma(CH_2)$ represents the methylene carbons (C_4,C_7,C_{11}) [33.3 ppm]
γ(CH) represents the methinyl carbons (C_5,C_8,C_{10}) [47.6 ppm]
b) Relaxation times given in seconds
c) Correlation times given in picoseconds

Table II. ^{13}C NMR Relaxation and Correlation Times in THC-CH_2OH

T (°C)	Carbon[a]	θ	T_1[b]	NOE	T_{1DD}[b]	τ_c[c]
46	β	53°	9.69	2.75	11.01	4.23
	$\gamma(CH_2)$	47.3°,132.7°	5.63	2.99	5.63	4.14
	$\gamma(CH)$	127°	9.75	2.68	11.54	4.04
	δ	0	8.22	2.85	8.83	5.27
34	β	53°	8.08	2.78	9.02	5.16
	$\gamma(CH_2)$	47.3°,132.7°	4.60	2.99	4.60	5.07
	$\gamma(CH)$	127°	8.08	2.71	9.39	4.96
	δ	0	6.83	2.87	7.26	6.41
21	β	53°	6.54	2.80	7.22	6.45
	$\gamma(CH_2)$	47.3°,132.7°	3.63	2.99	3.63	6.41
	$\gamma(CH)$	127°	6.48	2.75	7.36	6.33
	δ	0	5.50	2.88	5.82	8.01
10	β	53°	5.38	2.82	5.88	7.92
	$\gamma(CH_2)$	47.3°,132.7°	2.92	2.99	2.92	7.97
	$\gamma(CH)$	127°	5.29	2.78	5.91	7.88
	δ	0	4.50	2.89	4.73	9.84
-9	β	53°	3.69	2.85	3.97	11.74
	$\gamma(CH_2)$	47.3°,132.7°	1.92	2.99	1.92	12.11
	$\gamma(CH)$	127°	3.58	2.84	3.87	12.04
	δ	0	3.07	2.91	3.20	14.57
-21	β	53°	2.83	2.88	2.99	15.56
	$\gamma(CH_2)$	47.3°,132.7°	1.43	2.98	1.43	16.24
	$\gamma(CH)$	127°	2.72	2.87	2.89	16.10
	δ	0	2.34	2.92	2.42	19.22
-42	β	53°	1.66	0.02	1.72	27.01
	$\gamma(CH_2)$	47.3°,132.7°	0.79	2.98	0.79	29.37
	$\gamma(CH)$	127°	1.56	2.93	1.61	29.01
	δ	0	1.36	2.94	1.40	33.40

a) β represents the methinyl carbons (C_1,C_3,C_6) [49.8 ppm]
$\gamma(CH_2)$ represents the methylene carbons (C_4,C_7,C_{11}) [32.2 ppm]
$\gamma(CH)$ represents the methinyl carbons (C_5,C_8,C_{10}) [47.4 ppm]
δ represents the apical carbon (C_9) [41.7 ppm]
b) Relaxation times given in seconds
c) Correlation times given in picoseconds

Table III. ^{13}C NMR Relaxation and Correlation Times in THC-$CONH_2$

T (°C)	Carbon[a]	θ	T_1[b]	NOE	T_{1DD}[b]	τ_c[c]
46	β	53°	8.52	2.77	9.58	4.86
	$\gamma(CH_2)$	47.3°,132.7°	4.76	2.99	4.76	4.89
	$\gamma(CH)$	127°	8.63	2.73	9.89	4.71
	δ	0	4.11	2.56	5.24	8.89
34	β	53°	7.35	2.79	8.17	5.70
	$\gamma(CH_2)$	47.3°,132.7°	4.03	2.99	4.03	5.78
	$\gamma(CH)$	127°	7.42	2.75	8.44	5.52
	δ	0	3.32	2.62	4.07	11.43
22	β	53°	6.27	2.81	6.88	6.77
	$\gamma(CH_2)$	47.3°,132.7°	3.36	2.99	3.36	6.93
	$\gamma(CH)$	127°	6.30	2.76	7.10	6.55
	δ	0	2.63	2.68	3.12	14.95
9	β	53°	5.20	2.83	5.63	8.27
	$\gamma(CH_2)$	47.3°,132.7°	2.72	2.99	2.72	8.57
	$\gamma(CH)$	127°	5.19	2.78	5.81	8.02
	δ	0	2.00	2.74	2.28	20.40
-5	β	53°	4.16	2.86	4.45	10.47
	$\gamma(CH_2)$	47.3°,132.7°	2.11	2.99	2.11	11.04
	$\gamma(CH)$	127°	4.13	2.79	4.58	10.17
	δ	0	1.44	2.81	1.59	29.34
-25	β	53°	2.90	2.90	3.04	15.33
	$\gamma(CH_2)$	47.3°,132.7°	1.40	2.99	1.40	16.66
	$\gamma(CH)$	127°	2.85	2.82	3.12	14.93
	δ	0	0.85	2.90	0.89	52.41
-45	β	53°	1.89	2.93	1.95	23.89
	$\gamma(CH_2)$	47.3°,132.7°	0.86	2.99	0.86	26.98
	$\gamma(CH)$	127°	1.84	2.84	1.99	23.40
	δ	0	0.46	2.99	0.46	101.63

a) β represents the methinyl carbons (C_1,C_3,C_6) [53.7 ppm]
$\gamma(CH_2)$ represents the methylene carbons (C_4,C_7,C_{11}) [33.5 ppm]
$\gamma(CH)$ represents the methinyl carbons (C_5,C_8,C_{10}) [48.3 ppm]
δ represents the apical carbon (C_9) [44.4 ppm]
b) Relaxation times given in seconds
c) Correlation times given in picoseconds

Table IV. ^{13}C NMR Relaxation and Correlation Times in THC-$COOCH_3$

T (°C)	Carbon[a]	θ	T_1[b]	NOE	T_{1DD}[b]	τ_C[c]
46	β	53°	8.61	2.57	10.90	4.27
	$\gamma(CH_2)$	47.3°,132.7°	4.68	2.99	4.68	4.98
	$\gamma(CH)$	127°	8.42	2.73	9.68	4.81
	δ	0	5.30	2.71	6.16	7.56
32	β	53°	7.35	2.63	8.96	5.19
	$\gamma(CH_2)$	47.3°,132.7°	3.90	2.99	3.90	5.97
	$\gamma(CH)$	127°	7.20	2.76	8.13	5.73
	δ	0	4.32	2.75	4.91	9.49
22	β	53°	6.51	2.67	7.77	5.99
	$\gamma(CH_2)$	47.3°,132.7°	3.39	2.99	3.39	6.87
	$\gamma(CH)$	127°	6.38	2.79	7.11	6.55
	δ	0	3.68	2.78	4.12	11.30
10	β	53°	5.57	2.71	6.48	7.19
	$\gamma(CH_2)$	47.3°,132.7°	2.83	2.99	2.83	8.22
	$\gamma(CH)$	127°	5.46	2.81	6.00	7.77
	δ	0	3.00	2.81	3.30	14.14
-5	β	53°	4.48	2.77	5.03	9.25
	$\gamma(CH_2)$	47.3°,132.7°	2.20	2.99	2.20	10.58
	$\gamma(CH)$	127°	4.41	2.85	4.74	9.83
	δ	0	2.26	2.85	2.43	19.18
-25	β	53°	3.23	2.85	3.47	13.43
	$\gamma(CH_2)$	47.3°,132.7°	1.51	2.99	1.51	15.41
	$\gamma(CH)$	127°	3.18	2.89	3.34	13.95
	δ	0	1.48	2.91	1.54	30.25
-45	β	53°	2.19	2.93	2.25	20.65
	$\gamma(CH_2)$	47.3°,132.7°	0.97	2.99	0.97	24.13
	$\gamma(CH)$	127°	2.16	2.94	2.21	21.04
	δ	0	0.89	2.97	0.90	51.76

a) β represents the methinyl carbons (C_1,C_3,C_6) [52.9 ppm]
$\gamma(CH_2)$ represents the methylene carbons (C_4,C_7,C_{11}) [32.7 ppm]
$\gamma(CH)$ represents the methinyl carbons (C_5,C_8,C_{10}) [47.4 ppm]
δ represents the apical carbon (C_9) [41.0 ppm]
b) Relaxation times given in seconds
c) Correlation times given in picoseconds

Table V. ^{13}C NMR Relaxation and Correlation Times in THC-COOH

T (°C)	Carbon[a]	θ	T_1[b]	NOE	T_{1DD}[b]	τ_c[c]
46	β	53°	6.22	2.62	7.63	6.10
	$\gamma(CH_2)$	47.3°,132.7°	2.96	2.98	2.97	7.84
	$\gamma(CH)$	127°	6.29	2.68	7.44	6.26
	δ	0	1.29	2.92	1.34	34.87
32	β	53°	5.32	2.68	6.30	7.40
	$\gamma(CH_2)$	47.3°,132.7°	2.45	2.98	2.46	9.48
	$\gamma(CH)$	127°	5.23	2.73	6.01	7.75
	δ	0	1.05	2.92	1.09	42.74
20	β	53°	4.37	2.72	5.05	9.22
	$\gamma(CH_2)$	47.3°,132.7°	2.06	2.98	2.06	11.28
	$\gamma(CH)$	127°	4.41	2.77	4.95	9.40
	δ	0	0.88	2.92	0.91	51.28
10	β	53°	3.74	2.77	4.21	11.05
	$\gamma(CH_2)$	47.3°,132.7°	1.77	2.99	1.77	13.14
	$\gamma(CH)$	127°	3.79	2.81	4.17	11.17
	δ	0	0.74	2.92	0.77	60.83
-5	β	53°	2.91	2.83	3.17	14.70
	$\gamma(CH_2)$	47.3°,132.7°	1.37	2.99	1.37	16.98
	$\gamma(CH)$	127°	2.94	2.86	3.14	14.83
	δ	0	0.56	2.92	0.58	80.13
-25	β	53°	1.98	2.91	2.06	22.56
	$\gamma(CH_2)$	47.3°,132.7°	0.93	2.99	0.93	25.12
	$\gamma(CH)$	127°	2.01	2.93	2.07	22.54
	δ	0	0.37	2.92	0.38	121.57
-42	β	53°	1.36	2.98	1.37	34.03
	$\gamma(CH_2)$	47.3°,132.7°	0.63	2.99	0.63	36.84
	$\gamma(CH)$	127°	1.38	2.99	1.38	33.75
	δ	0	0.24	2.91	0.25	183.75

a) β represents the methinyl carbons (C_1,C_3,C_6) [53.0 ppm]
$\gamma(CH_2)$ represents the methylene carbons (C_4,C_7,C_{11}) [32.7 ppm]
$\gamma(CH)$ represents the methinyl carbons (C_5,C_8,C_{10}) [47.4 ppm]
δ represents the apical carbon (C_9) [40.9 ppm]
b) Relaxation times given in seconds
c) Correlation times given in picoseconds

function of temperature (in $CHCl_3$ solvent) are shown in Tables I to V. The values of $D_\perp$ for **1a** - **1e** are shown in Table VI-A. Experimental and calculated diffusional constants of **1a** - **1e** are compared in Table VII.

The tumbling rates of compounds **1b** - **1e** are slower than those of the parent hydrocarbon, **1a**, since the diameters of the principal axes (σ_a in Table VII) of **1b-1e** are substantially greater than the corresponding diameters of **1a**, as one may expect. The rotation of the principal axis in **1b-1e** requires greater solvent displacement than in **1a**, therefore resulting in a larger frictional torque, which retards this motion in the substituted THCs relative to that in the parent hydrocarbon (**1a**). Some specific intermolecular interactions must be considered when interpreting the experimental results, because the relative rotational rates of **1b-1e** do not correlate well with their long-axis diameters; for example, the σ_a of **1c** has the largest value but **1c** rotates faster than does either **1b** or **1e**. The tumbling rate of **1b** is much slower than that of the other four substituted THCs. That carboxylic acids spontaneously form hydrogen bonded dimers in the gas and in nonpolar solvent is well documented.[15,16] The low $D_\perp$ value of THC-COOH is a manifestation of the formation of stable hydrogen bonded dimers. This fact provides reasonable support that the low $D_\perp$ of **1b** is due to its dimeric association, which has a longer time scale than the

Table VI. Reorientational Diffusion Coefficients in Substituted Trishomocubanes[a]

A. Perpendicular ($D_\perp$)

T (°C)	THC	THC-CH_2OH	THC-$CONH_2$	THC-$COOCH_3$	THC-COOH
46	71	32	19	22	4.8
34	63	26	15	18	3.9
22	53	21	11	15	3.3
10	47	17	8.2	12	2.7
-5	38	11	5.7	8.7	2.1
-22	30	8.7	3.2	5.5	1.4
-42	21	5.0	1.6	3.3	0.9
Ea (kcal/mol)	2.0	3.1	3.9	3.0	2.8

B. Parallel ($D_\parallel$)

T (°C)	THC	THC-CH_2OH	THC-$CONH_2$	THC-$COOCH_3$	COOH
46	87	64	85	77	103
34	79	51	78	67	84
22	67	40	70	60	69
10	61	32	61	53	59
-5	51	21	51	43	45
-22	40	15	38	32	30
-42	29	8.1	26	25	20
Ea (kcal/mol)	1.8	3.4	1.9	1.8	2.7

a) Diffusion coefficients are given in units of $ns^{-1}(10^9\ s^{-1})$

Table VII. Comparison of Experimental and Calculated Diffusion Coefficients in Substituted Trishomocubanes at 22 °C[a]

	THC	THC-CH_2OH	THC-$CONH_2$	THC-$COOCH_3$	THC-COOH[b] (Monomer)	THC-COOH[b] (Dimer)
$D_\perp$(Exp)	53	21	11	15	3.3	3.3
$D_\perp$(Stick)	5.0	3.9	3.8	3.5	3.8	1.4
$D_\perp$(Slip)	519	441	310	138	225	5.4
$D_\perp$(μ-Visc)	30	12	11	8.5	11	1.2
σ_a	7.12 Å	9.03 Å	9.21 Å	9.83 Å	9.17 Å	16.63 Å
$D_\parallel$(Exp)	67	40	70	60	69	69
$D_\parallel$(Stick)	5.2	4.0	4.0	3.7	4.0	2.1
$D_\parallel$(Slip)	186	186	186	186	186	186
$D_\parallel$(μ-Visc)	18	18	18	18	18	18
σ_b	8.05 Å	8.05 Å	8.05 Å	8.05 Å	8.05 Å	8.05 Å

a) Diffusion coefficients are given in units of $ns^{-1}(10^9\ s^{-1})$
b) Theoretical coefficients for the acid derivative were calculated assuming both monomeric and dimeric structures

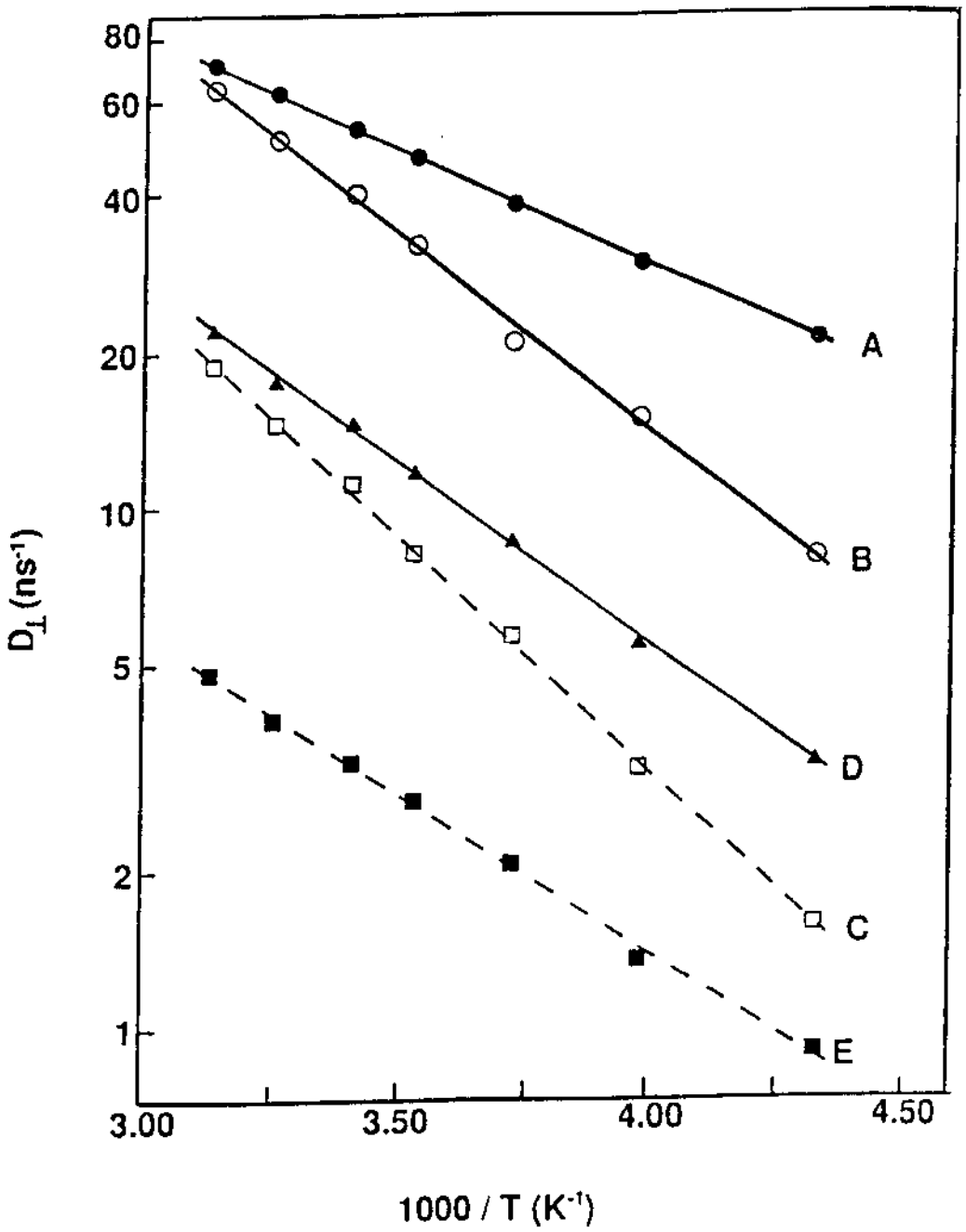

Figure 7. Perpendicular ('Tumbling') Diffusion Coefficients in Substituted Trishomocubanes.
(A) THC - Filled circles and solid line;
(B) THC-CH_2OH - Open circles and solid line;
(C) THC-$CONH_2$ - Open squares and dashed line;
(D) THC-$COOCH_3$ - Filled triangles and solid line;
(E) THC-COOH - Filled squares and dashed line.

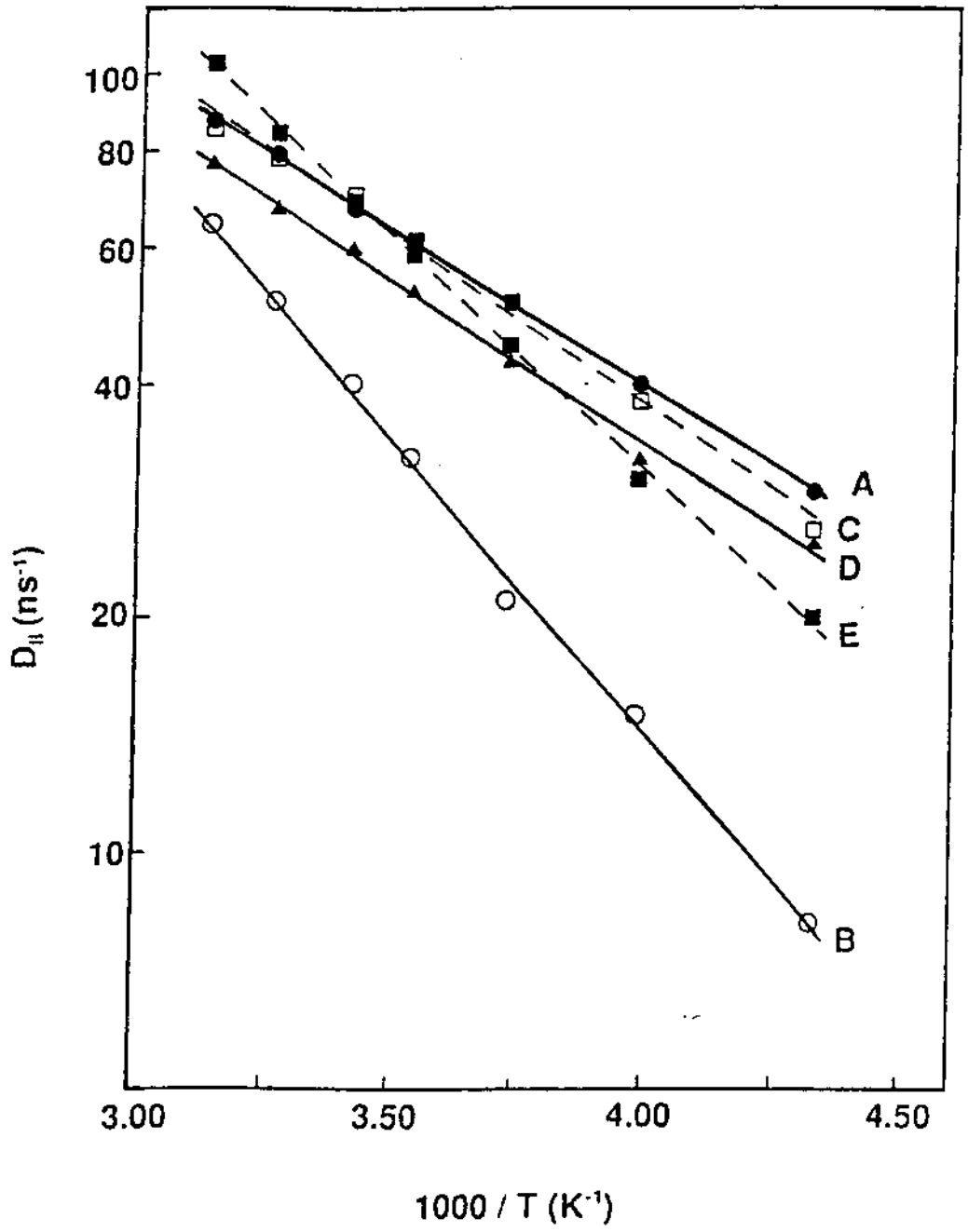

Figure 8. Parallel ('Spinning') Diffusion Coefficients in Sunstituted Trishomocubanes
(A) THC - Filled circles and solid line;
(B) THC-CH_2OH - Open circles and solid line;
(C) THC-$CONH_2$ - Open squares and dashed line;
(D) THC-$COOCH_3$ - Filled triangles and solid line;
(E) THC-COOH -. Filled squares and dashed line.

period of rotation (0.2-1.0 ns).

The formation of intermolecular (peptide-like) hydrogen bonds can be the cause of the slower tumbling rate of **1e** than what would be expected on the basis of the length of its major axis. That this type of intermolecular association in $CHCl_3$ is shorter-lived in **1e** than in **1b** is evident by the fact that $D_\perp$ for **1e** is much greater than that for **1b**. The E_a's in stable complexes are usually comparable to those in non-associative solvents.[16] An increase in reorientational activation energy occurs when intermolecular hydrogen bonds are short-lived and are readily broken during the course of molecular rotation.[17] The higher E_a for $D_\perp$ in **1e** than in any of the other THCs studied (Table VI-A) is an additional evidence of the transient nature for the hydrogen-bonded association in **1e**.

The $D_\parallel$'s of **1a-1e** are shown in Table VI-B and in Figure 7. The trends in $D_\parallel$ in the substituted THCs studied, in contrast to the results for $D_\perp$, are very similar to those in the parent hydrocarbon (**1a**). This result indicates that the substitution at C(2) in **1a** has no significant effect on the spinning rate about the principal axis and that there is almost no barrier to rotation about the C(2)-X bond in 2-substituted THCs. The lower $D_\parallel$ values in **1d** than those in the other THCs (see Figure 8) provide evidence for the existence of a larger (steric) barrier to internal rotation about the C(2)-CH_2OH bond in **1d** as compared to the

corresponding process in **1b**, **1c**, and **1e**. A calculation of the internuclear distances of **1d** as a function of torsion angle (using the MOBY molecular modeling program) shows that the hydroxymethyl methylene hydrogen atoms in **1d** must approach the hydrogens which are bonded to C(1), C(3), and C(6) within 2.2 Å. This distance is much less than the sum of their van der Waal radii, 2.4 Å,[18] indicating that a substantial steric barrier to internal rotation can be expected in **1d**.

D. Comparison with Theoretical Predictions

In an attempt to determine rotational diffusion constants which characterize the molecular reorientation in liquid systems, several diffusion models have been developed in the past years. It may be possible to give *a priori* predictions[19] of the rates of molecular rotation of symmetric top molecules in solution if we can compare the experimental diffusion coefficients for THC compounds with those calculated from theoretical models of reorientational dynamics. The experimental and calculated values of $D_{\perp}$ and $D_{\parallel}$ for **1a-1e** at 22°C are given in Table VII.

The "stick" model, the oldest formalism for reorientation, was first developed by Stokes[20] for spheres and then was extended substantially by Perrin[21] to include ellipsoidal molecules. The stick model assumes that the solvent sticks to the surface of the molecule, thus creating

a viscous drag, which retards its rotation. The values of $D_{\perp}$(Stick), as shown in Table VII, are three to eleven times lower than the experimental values except in **1b**. The calculated $D_{\parallel}$(Stick) values agree even more poorly with experiment than do the corresponding $D_{\perp}$(Stick) values. $D_{\parallel}$(Stick) is between ten and thirty times lower than experiment.

The "slip" model was developed by Hu and Zwanzig,[22] in which solvent molecules are assumed to glide smoothly past the surface of the solvent. In the slip model limit, a spherical molecule experiences no opposing force and is expected to rotate as rapidly in solution as does a free rotor in the gas phase. For ellipsoidal molecules (e.g., THCs **1b-1e**), the tumbling of the molecules in solution requires the displacement of solvent, whereas spinning about the principal axis can proceed unimpeded. The calculated $D_{\perp}$ values from the slip model are one to two orders of magnitude greater than those derived from the experiment, as shown in Table VII, and the $D_{\parallel}$(Slip) is three to five times greater than the $D_{\parallel}$(Expt).

Gierer and Wirtz[23] introduced a reorientation model, the "microviscosity" model, which is intermediate between the stick and slip limits. The microviscosity model assumes that solvent binds tightly to the surface of the solute. But, the contact area between solvent and solute molecules is reduced due to the fact that solvent and solute molecules

are comparable in size. As shown in Table VII, the microviscosity model predicts $D_{\perp}$, which agrees qualitatively with experiment within a factor of 2. The poor agreement between $D_{\parallel}(\mu\text{-visc})$ and $D_{\parallel}(\text{Expt})$ indicates that the spinning of these molecules in $CHCl_3$ solution conforms more closely to the predictions based on the limiting slip model.

E. Summary and Conclusions

D_3-Trishomocubane (THC, **1a**) and four 2-substituted THCs (**1b-1e**) were synthesized (by Dr. Marchand's post-doctoral associates) for the ^{13}C NMR relaxation study. ^{13}C NMR spin-lattice relaxation time (T_1) and nuclear Overhauser enhancements of various skeletal carbon atoms in these substrates were obtained experimentally, and these quantities were used to determine the perpendicular and parallel reorientational diffusion coefficients ($D_{\perp}$ and $D_{\parallel}$) for **1a-1e** in $CHCl_3$ solution as a function of temperature.

The molecular tumbling rates ($D_{\perp}$) of **1b-1e** all are markedly slower than that of the parent hydrocarbon, **1a**. The relative magnitudes of $D_{\perp}$ in **1b-1e** provide convincing evidence for the formation of long-lived hydrogen-bonded dimers in **1b** and of more transient hydrogen-bonded association complexes in **1e**. In contrast to the perpendicular diffusion coefficients, values of $D_{\parallel}$ in **1b**, **1c** and **1e** were equal to the corresponding values in **1a**, thereby indicating the existence of a negligible barrier to the

rotation about the C(2)-X bond in these 2-substituted THCs. The slower spinning rate observed in **1d** can be attributed to the existence of a steric barrier to the internal rotation in this compound.

The application of the classical "stick" and "slip" models of reorientational dynamics in solution afforded calculated diffusion coefficient values that were far lower and higher, respectively, than the corresponding experimental values. The calculated values of $D_{\perp}$, which were obtained by employing the microviscosity model, were in good qualitative agreement with experiment. However, this theory, failed to provide accurate estimates of the spinning rate ($D_{\parallel}$) of **1b-1e**.

CHAPTER REFERENCES

1. Relevant reviews on applications of NMR relaxation to rotational dynamics include: (a) Wright, D. A.; Axelson, D. E.; Levy, G. C. in Topics in Carbon-13 NMR; Levy, G. C. Ed.; Wiley: New York, **1979**; Vol. 3, p 103. (b) Boere, R. T.; Kidd, R. G. Annu. Rep. NMR Spectrosc. **1982**, 13, 319. (c) Versmold, H. NATO ASI Ser., Ser. C **1984**, No. 135, 309.

2. Dolle, A.; Bluhm, T. Prog. NMR Spectrosc. **1989**, 21, 175.

3. Marchand, A. P. In Advances in Theoretically Interesting Molecules; Thummel, R. P., Ed.; JAI: Greenwich, CT; Vol. 1, **1989**, pp. 357-399.

4. Approximate sample concentrations: **1a**, 0.8M; **1b**, 0.6M; **1c**, 0.6M; **1d**, 0.6M; **1e**, 0.2M

5. Martin, M. L.; Delpuech, J. J.; Martin, G. J. Practical NMR Spectroscopy; Heyden, London, **1980**; Chapter 7.

6. Rodriguez, A. A.; Chen, S. J. H.; Schwartz, M. J. Magn. Reson. **1987**, 74, 114.

7. Martin, M. L.; Delpuech, J. J.; Martin, G. J. Practical NMR Spectroscopy; Heyden, London, **1980**; Chapter 6.

8. (a) Noggle, J. H.; Schirmer, R. E. The Nuclear Overhauser Effect; Academic Press: New York, **1971**. (b) Neuhaus, D. Williamson, M. The Nuclear Overhauser Effect in Sterochemistry and Conformational Analysis; VCH Publishers, New York, **1989**.

9. Becker, E. D. High Resolution NMR: Theory and Applications, 2nd ed.; Academic: New York, **1980**; Chapter 8.

10. Woessner, D. E. J. Chem. Phys. **1962**, 37, 647.

11. MOBY: Molecular Modeling on the PC, Version 1.4; Springer-Verlag: Berlin, **1991**.

12. Watson, W. H.; Nagl, A.; Marchand, A. P.; Vidyasagar, V. Acta Crystallogr., Sect. C: Cryst. Struct. Commun. **1989**, C45, 1770.

13. Dewar, M. J. S.; Zoebisch, E. G.; Healy, E. F.; Stewart, J. J. P. J. Am. Chem. Soc. **1985**, 107, 3902.

14. Burkert, U. and Allinger, N. L. Molecular Mechanics, American Chemical Society, Washington, D.C., **1982**.

15. (a) Beierbeck, H.; Martino, R. Saunders, J. K. Can. J. Chem. **1979**, 57, 1224. (b) Craik, D. J.; Adcock, W.; Levy, G. C. Magn. Reson. Chem. **1986**, 24, 783.

16. Levy, G. C.; Terpstra, D. Org. Magn. Reson. **1976**, 8, 658.

17. (a) Levy, G. C.; Holak, T. A.; Steigel, A. J. J. Am. Chem. Soc. **1976**, 98, 495. (b) Edlund, U.; Holloway, C. E.; Levy, G. C. J. Am. Chem. Soc. **1976**, 98, 5069.

18. Bondi, A. J. Phys. Chem. **1964**, 68, 441.

19. (a) Chen, A. F. T.; Wang, S. P.; Schwartz, M. Magn. Reson. Chem. **1988**, 26, 675. (b) Rodriguez, A. A.; Chen, A. F. T.; Schwartz, M. J. Mol. Lig. **1988**, 37, 117.

20. (a) Stokes, G. Trans. Gambridge Philos. Soc. **1856**, 9, 5. (b) Debye, P. Polar Molecules; Dover Press: New York **1929**.

21. Perrin, E. J. Chem. Radium, **1934**, 5, 497.

22. Hu, C. M.; Zwanzig, R. J. Chem. Phys., **1974**, 60, 4354.

23. Gierer, A.; Wirtz, K. Zeit. Naturforsch., **1953**, A8, 532.

CHAPTER V

RAMAN & NMR STUDY OF PARALLEL REORIENTATIONAL DIFFUSION IN CH_3NO_2

A. Introduction

The Raman bandwidth analysis of double degenerate vibrations has proven to be a useful method in determining the parallel, 'spinning', reorientational diffusion coefficients, $D_{\parallel}$s, in molecules of D_{3h}[1,2] and D_{6h}[3-6] symmetry. Due to the more complex dependence of the vibrational bandshape of E modes in C_{3v} molecules on $D_{\perp}$, $D_{\parallel}$, and Δ_v (the contribution due to the vibrational relaxation), the initial attempts to investigate the parallel rotation in this important class of molecules were unsuccessful.

A method has been developed in our lab, in which the degenerate vibrations of C_{3v} molecules are analyzed to extract parallel diffusion coefficients in systems containing methyl rotors. This method has proven to be physically realistic in obtaining parallel diffusion coefficients in several systems with methyl rotors.[7-10] In order to determine whether this methodology can be applied to the methyl group reorientation in molecules with symmetry lower than C_{3v}, the Raman bandwidths of ν_1 (CD_3 symmetric stretch) and ν_7 (CD_3 antisymmetric stretch) vibrations in

nitromethane-d_3 have been measured as a function of temperature in the liquid phase. Alternatively, for the purpose of comparing with the Raman results, deuterium NMR relaxation times were also measured to obtain $D_{\|}$ in CD_3NO_2.

B. Experimental

1. Sample Preparation

Nitromethane-d_3 was used as received. Raman samples were sealed in capillary melting point tubes. Nitromethane was transfered to a 10 mm NMR sample tube, degassed by three freeze-pump-thaw cycles and flame sealed under vacuum.

2. Raman Spectrum & NMR Relaxation Times Measurements

Raman spectra were acquired with a spectroscopic slitwidth of 4.3 cm^{-1} and a frequency increment of 0.5 cm^{-1} on a Spex 14018 laser Raman spectrometer, with an argon-ion laser (4880Å) as the irradiation source. Polarized and depolarized spectra of ν_1 (centered at 2190 cm^{-1}) were measured between 2160 and 2215 cm^{-1} and the iotropic spectrum was calculated from the standard expression:

$$I_{iso}(\omega) = I_{pol}(\omega) - (4/3)I_{depol}(\omega) \qquad (57)$$

The isotropic vibrational relaxation linewidth, $\Delta_v(\nu_1)$ in Table VIII, was determined by a fit of the isotorpic spectrum by a Lorentzian bandshape. The depolarized spectra

of ν_7 (at 2315 cm^{-1}) were measured between 2145 cm^{-1} and 2490 cm^{-1}. The spectra of the degenerate mode were fitted by a model consisting of the sum of two Lorentzians with the same center but different heights and widths, $\Delta_1^{(2)}$ and $\Delta_2^{(2)}$. The greater linewidth, $\Delta_1^{(2)}$, is actually broadened by a non-reorientational (probably due to collisional) process, and can not be used in the analysis.[11,12] The narrower bandwidths were measured as a function of temperature. The results are listed in Table VIII under $[\Delta_1^{(2)}(\nu_7)]$. All measurements were repeated at least three times at each temperature; the results in Table VIII are the average of the measurements.

Deuterium spin-lattice relaxation times were measured at $\nu_o(^2H)$=46.05 MHz on a Varian VXR-300 FT-NMR spectrometer. The probe temperature was regulated by high pressure liquid nitrogen boil-off or heated air flow and measured with a thermocouple that was calibrated by using an NMR thermometer. Relaxation times were determined by using the standard inverse recovery pulse sequence,[13] with a pulse delay, $D > 5T_1$, and n=8 transients at each of 10 τ values plus $\tau \to \infty$. T_1 values were calculated via non-linear regression using a three-parameter (M_o, $\cos\theta$, T_1) magnetization equation (Eq. [97]).[14] At least three values of the relaxation time were obtained at each temperature. The average values of $T_1(^2H)$ and the mean deviations between runs are given in Table VIII.

Table VIII. Temperature Dependence of Bandwidths and Relaxation Times in Nitromethane-d_3[a]

T	$\Delta_v(\nu_1)$	$\Delta_1^{(2)}(\nu_7)$	$T_1(^2H)$	τ_1(Diel)[b]	$T_1(^{14}N)$[c]
261 K	8.2 cm^{-1} (0.1)	23.2 cm^{-1} (0.7)	4.22 s (0.04)	3.9 ps	13.9 ms
280	8.0 (0.1)	25. (1.)	4.9 (0.1)	3.2	17.9
296	7.8 (0.1)	24.1 (0.4)	5.61 (0.05)	2.8	21.5
313	8.65 (0.00)	30. (1.)	6.8 (0.1)	2.4	25.6
334	9.28 (0.11)	34.5 (2.5)	7.8 (0.2)	2.1	31.0

a) Quantities in parentheses represent the mean deviation between runs.
b) Interpolated from the results in ref. [16].
c) Calculated from the data in ref. [18].

3. Data Acquisition and Analysis

In nitromethane, the dipole moment lies along the principal axis. Therefore, the dielectric relaxation time (τ_1(diel)) can be used to derive the diffusion constant via the relation: $\tau_1 = [2D_\perp]^{-1}$.[15,16] The molecular (τ_1) dielectric relaxation times in neat nitromethane, as measured by Chandra and Nata,[17] were adopted and fitted by the Arrhenius equation. Values for τ_1 were calculated at the temperatures were utilized in our study. The results are shown in the fifth column of Table VIII. The values of the tumbling diffusion coefficient, obtained from dielectric relaxation, are given in Table IX.

If the principal axis of the ^{14}N electric field gradient (efg) tensor in nitromethane is parallel to the principal molecular axis, then, $D_\perp$ can be calculated from the ^{14}N-NMR relaxation time [$T_1(^{14}N)$]. We have also adopted the results of a reported ^{14}N relaxation time study by Moniz and Gutowsky[18] in nitromethane, T_1=22 ms at 25°C and E_a=1.9 kcal/mol. These data were used to generate $T_1(^{14}N)$ as a function of temperature (Table VIII, the last column). Further, these $T_1(^{14}N)$ data were used to calculate τ_c via equation (26). In the third column of Table IX, the displayed $D_\perp$ were derived via $D_\perp = [6\tau_c]^{-1}$ by using $\chi(^{14}N)$=1.695 MHz and ξ=0.424 in nitromethane as reported by Subbarao and his coworkers.[19]

The Raman bandshapes of ν_1 (CD_3 symmetric stretch) and

ν_7 (CD_3 antisymmetric stretch) vibrations in nitromethane-d_3 have been measured as a function of temperature in the liquid phase in order to test whether our methodology is applicable to the study of methyl group reorientation in molecules with symmetry lower than C_{3v}. The narrower of the two Lorentzian components of the Raman spectra of degenerate E mode, $\Delta_1^{(2)}$, was used to derive $D_\parallel$ via the relation:

$$\Delta_1^{(2)} = \Delta_v + (\pi C)^{-1}[5D_\perp + D_\parallel] \qquad (93a)$$

The quantity Δ_v, which can not be measured directly, was estimated from the isotropic (vibrational reorientation) bandwidth of an equivalent A_1 vibration via a method suggested by Tanabe.[1] The results are shown in the first two columns of Table VIII.

With $D_\perp$(diel), $\Delta_1^{(2)}$, and Δ_v, the spinning rates of methyl group can be derived and are shown as $D_\parallel$(Ram) in Table IX.

The deuterium spin-lattice (T_1) NMR relaxation times were also measured in order to obtain an alternative determination of spinning diffusion coefficient, $D_\parallel$, in CD_3NO_2. However, the calculation of τ_c via eq. (26) requires a knowledge of the deuterium QCC [$\chi(^2H)$]. The literature[20] values of the $\chi(^2H)$ ranged from 128 to 161 KHz. These two limiting values of $\chi(^2H)$ were used in eq. (26) to calculate $D_\parallel$. The results are listed in Table IX as

Table IX. Temperature Dependence of Reorientational Diffusion Coefficients in Nitromethane-d_3[a,b]

T	$D_\perp$(Diel)	$D_\perp(^{14}N)$	$D_\perp$(HKW)	$D_\parallel$(Ram)	$D_\parallel(^2H)_{MAX}$	$D_\parallel(^2H)_{MIN}$	$D_\parallel$(FR)
261	12.8	10.5	11.0	85 (11)	58 (02)	23 (01)	133
280	15.6	13.4	13.4	90 (16)	65 (04)	26 (02)	138
296	18.0	16.2	15.8	71 (07)	75 (05)	30 (01)	142
313	20.6	19.2	18.5	107 (14)	95 (04)	38 (02)	146
334	23.9	23.5	22.2	127 (37)	109 (08)	43 (03)	151
E_a [kcal/mol]	1.5	1.9	1.7	0.9	1.6	1.6	0.3

a) Diffusion coefficients are given in units of 10^{10} s^{-1}.
b) Quantities in parentheses represent calculated standard deviations in $D_\parallel$.

$D_{\parallel}(^2H)_{max}$ and $D_{\parallel}(^2H)_{min}$, which were calculated from $\chi(^2H)$= 161 KHz and 128 KHz respectively.

C. Results and Discussion

The degenerate CD_3 stretching mode may split into B_1 and B_2 components. The CD_3NO_2 Raman spectrum of this vibration shows no evidence of any splitting because of the lack of appreciable coupling of the CD_3 stretching vibrations to any of the NO_2 modes, which are of significantly lower frequency.[20,21] The measurement of Raman bandwidths of A_1 vibrations has been a routine procedure for the determination of the 'tumbling' rotational diffusion constants in symmetric top molecules.[15,16] It appears resonable to hope that the analysis of A_1 vibrations not directly involving the NO_2 group might yield realistic values for $D_{\perp}$, though nitromethane is not a symmetric-top molecule. The attempts to calculate $D_{\perp}$ values from the ν_1 (CD_3 symmetric stretch) and ν_4(C-N stretch) modes in nitromethane were unsuccessful, due to a combination of low depolarization ratio and overlap with neighbouring bands.

The dielectric relaxation time measurement may be used to calculate $D_{\perp}$ in nitromethane since the dipole moment lies along the principal axis. The utilization of Chandra et. al.'s data provided us the τ_1's at the temperature in our study. Further, these τ_1's were used to calculate $D_{\perp}$ values via the equation $D_{\perp} = [2\tau_1]^{-1}$.

An alternative method for $D_{\perp}$ calculation is from the

^{14}N NMR relaxation time [$T_1(^{14}N)$] when the principal axis of the ^{14}N electric field gradient (efg) is parallel to the principal molecular axis. The efg is not strictly required to lie along the principal molecular axis in nitromethane, since it has less than C_3 symmetry. If it were to lie at the same angle, θ, this would result in higher values for the apparent perpendicular diffusion coefficients. The relaxation time for a quadrupole nucleus is related to the reorientational correlation time, τ_c, by the expression:

$$\frac{1}{T_1} = \frac{1}{T_2} = \frac{3\pi^2}{10} \frac{2I+3}{I^2(2I-1)} \left(1+\frac{\xi^2}{3}\right) \chi^2 \tau_c(\theta) = \frac{3\pi^2}{2} \chi^2 \tau_c(\theta) \quad (26a)$$

In this equation, χ is the quadrupole coupling constant (in Hz), ξ is the electric field gradient in the vicinity of the nucleus and I is the nuclear spin quantum number, I=1 for both ^{14}N and ^{2}H, which leads to the final form of the above equation.

As shown in Table IX, the perpendicular diffusion coefficients determined from the dielectric and NMR relaxation are in very satisfactory agreement, lending support for the assumption that the principal axis of the ^{14}N efg is parallel to the symmetry axis.

The Gierer-Wirtz Microviscosity,[23] the Hu-Zwanzig,[24] and the Hynes-Kapral-Weinberg (HKW)[25] models of reorientational diffusion have been applied to obtain a

priori predictions of $D_\perp$ in nitromethane. As displayed in Table IX (the fourth column), the HKW model yields diffusion coefficients that are in virtually quantitative agreement with experiment. The theoretically predicted $D_\perp$ values by the GW and HZ models are substantially lower than the experimental results [$D_\perp(GW)=0.6-0.8D_\perp(exp)$ and $D_\perp(HZ)=0.3-0.4D_\perp(exp)$].

In previous work done in our laboratory,[7-10] it has been shown that the narrower of the two Lorentzian components ($\Delta_1^{(2)}$) of the Raman spectra of E bands in C_{3v} molecules may be used to determine $D_\parallel$ via the relation:

$$\Delta_1^{(2)} = \Delta_v + (\pi c)^{-1}[5D_\perp + D_\parallel] \qquad (93a)$$

where Δ_v is the contribution of vibrational relaxation to the bandwidth. This quantity, which cannot be measured directly, may be estimated from the isotropic (vibrational relaxation) bandwidth of an equivalent A_1 vibration via the relation, $\Delta_v(E)=\Delta_v(A_1)x[\omega(A_1)/\omega(E)]^2$, as originally suggested by Tanabe.[1] $\Delta_v(\nu_1)$ and the two experimental peak frequencies were used to calculate $\Delta_v(E)$. The measured linewidths [$\Delta_1^{(2)}$], Δ_v, and the $D_\perp$ obtained from the dielectric relaxation time have been used in equation (93a) to determine the parallel, spinning, diffusion coefficient as a function of temperature. This calculated results are listed in Table IX as $D_\parallel$(Raman). It is noted that this

quantity represents the spinning rate of the methyl group, rather than that of the whole molecule. This parameter has been labeled as D_{int} in some studies.[26]

NMR relaxation of a nucleus whose bond vector lies at an angle, θ, relative to the principal axis has been utilized as an alternative method to determine the spinning diffusion coefficient. The expression:[27]

$$\tau_c(\theta) = \frac{(1/4)(3\cos^2\theta - 1)^2}{6D_\perp} + \frac{3\sin^2\theta\cos^2\theta}{5D_\perp + D_\parallel} + \frac{(3/4)\sin^4\theta}{2D_\perp + 4D_\parallel} \quad (46)$$

presents the correlation time as a function of diffusion constants ($D_\parallel$ and $D_\perp$) and vector angle, θ. The requisite correlation time may be obtained from the deuterium relaxation, listed as $T_1(^2H)$ in Table VIII, because the C-D bond lies at θ=109.5° relative to the principal axis.[28] The calculation of τ_c via equation (26a) takes a knowledge of the deuterium QCC [$\chi(^2H)$]. Bjorholm and Jacobsen[20] have measured $\chi(^2H)$ for CD_3NO_2 in a variety of nematic liquid crystalline solvents. The result varied significantly between nematogens, ranging from 128 kHz to 161 kHz. Due to the near cyclindrical symmetry of the C-D bond, it is safe to assume that $\xi \approx 0$ in equation (26a). Therefore, these two limiting values have been applied to equation (26a) to calculate τ_c which, with $D_\perp$ derived from the dielectric relaxation, was fitted by equation 46 to determine the

parallel diffusion constant. The results are presented in Table IX. $D_{\parallel}(^2H)_{MAX}$ are values obtained using $\chi(^2H)$=161 kHz and $D_{\parallel}(^2H)_{MIN}$ are the results with $\chi(^2H)$=128 kHz. It is not surprising that there is a large variation between the two sets of diffusion coefficients since τ_c is inversely proportional to χ^2, as shown in equation (26a).

Hydrogen bond formation is one of the possible factors contributing to the vibrational band broadening.[29] This band broadening may be the cause of the $D_{\parallel}$'s derived from the Raman ν_7 bandwidth to be greater than the maximum values of $D_{\parallel}$ derived from $T_1(^2D)$ of nitromethane, which does not occur in either acetonitrile[9] or iodomethane.[7] The finding of this investigation provides further evidence for the existence of hydrogen bond interactions between methyl and nitro groups on neighboring molecules, which would be expected to slow the CD_3 spinning rate.

In earlier Raman and NMR studies of iodomethane[7] and acetonitrile,[9] it was found that the experimental values of $D_{\parallel}$ were close to those calculated from the Free Rotor model. In contrast, in this experiment, the $D_{\parallel}$'s derived from both Raman and NMR methods are far smaller than those calculated from the Free Rotor model, $D_{\parallel}(FR)$ in Table IX, indicating that the intermolecular self-association (hydrogen bond interactions) slows the spinning motion of nitromethane in the liquid phase. The intermolecular association in acetonitrile does not slow the spinning rate because the

interaction occurs between the C≡N groups on the neighboring molecules, and does not involve the methyl groups.

CHAPTER REFERENCES

1. Tanabe, K. Chem. Phys. Lett. **1979**, 6, 43.

2. Tanabe, K.; Hiraishi, J. Mol. Phys. **1980**, 39, 493.

3. Besnard, M.; Lascombe, J.; Nery, H. J. Phys.(paris), **1980**, 41, 723.

4. Lee H. I.; Kim, M. S. J. Raman Spectrosc. **1986**, 17, 269.

5. P. Yuan, P.; Chen, A. F. T.; Schwartz, M. J. Raman Spectrosc., **1989**, 20, 27.

6. Wang, S. P.; Chen, A. F. T.; Schwartz, M. Mol. Phys. **1989**, 65, 689.

7. Wang, S. P.; Yuan, P.; Schwartz, M.; J Raman Spectrosc. **1989**, 20, 339.

8. Wang, S. P.; Hu, W. P.; Schwartz, M.; Mol. Phys. **1989**, 68, 1125.

9. Yuan, P.; Schwartz, M. J. Chem. Soc., Faraday Trans. **1990**, 86, 593.

10. Wang, S. P.; Schwartz, M.; J. Phys. Chem. **1990**, 94, 2702.

11. Gompf, J.; Versmold, H.; Langer, H. Ber. Bunsenges. Phys. Chem. **1982**, 86, 1114.

12. Buckro, T. A.; Litowitz, T. A., J. Chem. Phys., **1971**, 54, 3846.

13. Martin, M. L.; Martin, G. J.; Delpuech, J. J. Practical NMR Spectroscopy, Chapter 7, Heyden, London 1980.

14. Rodriguez, A. A.; Chen, S. J. H.; Schwartz, M. J. Magn. Reson. **1987**, 74, 114.

15. Clarke, J. H. R.; Adv. Infrared Raman Spectrosc. **1978**, 4, 109.

16. Rothschild, W. G. Dynamics of Molecular Liquids, Wiley, New York, **1984**.

17. Chandra, S.; Nata, D. J. Chem. Phys. **1969**, 51, 5299.

18. Moniz, W. B.; Gutowsky, H. S. J. J. Chem. Phys. **1963**, 38, 115.

19. Subbarao, S. N.; Sauer, E. G.; Bray, P. J. Phys. Lett. **1973**, 42A, 461.

20. Bjorholm, T.; Jacobsen, J. P. Mol. Phys. **1984**, 51, 65.

21. Verderame, F. D.; Launon, J. A.; Harris, L. E.; Thomas, W. G.; Lucia, E. A. J. Chem. Phys. **1972**, 56, 2638.

22. Miller, P. J.; Block, S.; Piermarini, G. J. J. Phys. Chem. **1989**, 93, 462.

23. Gierer, A.; Wirtz, K. Z. Naturf. (a), **1953**, 8, 532.

24. Hu, C.-M.; Zwanzig, R. J. Chem. Phys. **1974**, 60, 4354.

25. Hynes, J. T., Kapral, R.; Weinberg, M. J. Chem. Phys. **1978**, 69, 2725.

26. Suchanski, W. Canepa, P. C., J. Magn. Reson. **1979**, 33, 389.

27. Woessner, D. E. J. Chem. Phys. **1962**, 37, 647.

28. Leipert, T. K.; Noggle, J. H.; Gillen, K. T. J. Magn. Reson. **1974**, 13, 158.

29. Knozinger, E.; Kollhoff, H.; Wittenbeck, R. Ber. Bunsenges. Phys. Chem. **1982**, 86, 929.

CHAPTER VI

REORIENTALIONAL DIFFUSION OF HFB/BENZENE BINARY LIQUID MIXTURES

A. Introduction

The fact that hexafluorobenzene and benzene form a 1:1 intermolecular complex in the solid phase is well documented.[1] In spite of the wealth of evidence from neutron scattering,[2] thermodynamics,[3] and X-ray studies of HFB/Benzene binary mixtures, the results of spectroscopic studies of HFB/Benzene solutions still remain ambiguous.[4-8] A typical example is the work done by Tanabe & Hiraishi.[7] In their analysis of a_{1g} vibrational modes of HFB and benzene, it was found that $D_{\perp}(B)$ decreases with the increase of HFB/Benzene solution viscosity but $D_{\perp}(HFB)$ displays anomalous results.

In order to have a more complete characterization of the reorientational dynamics in liquid HFB/Benzene mixtures, the measurements of several Raman a_{1g} and e_{2g} vibrations of HFB and benzene were carried out to determine their bandwidths as a function of binary mixture composition (the HFB mole fraction, X_{HFB}). The resulted bandwidths were then used to calculate the two diffusion coefficients, $D_{\parallel}$ and $D_{\perp}$, of HFB and benzene as a function of composition in solution.

Table X. Vibrational Frequencies Used in Experiment

Symmetry Type	Mode	Benzene	HFB
C-H or C-F symmetric stretch	$\nu_1(a_{1g})$	3064 cm^{-1}	1490 cm^{-1}
symmetry ring stretch	$\nu_2(a_{1g})$	991 cm^{-1}	559 cm^{-1}
C-H or C-F antisymm. stretch	$\nu_{15}(e_{2g})$	3051 cm^{-1}	1655 cm^{-1}

Table XI Concentration Dependence of Raman Bandwidths in Hexafluorobenzene/Benzene Mixtures[a,b,c,d]

	Hexafluorobenzene				Benzene			
X_{HFB}	$\Delta_{iso}(\nu_1)$	$\Delta_{iso}(\nu_2)$	$\Delta_{anis}(\nu_2)$	$\Delta_{anis}(\nu_{15})$	$\Delta_{iso}(\nu_1)$	$\Delta_{iso}(\nu_2)$	$\Delta_{anis}(\nu_2)$	$\Delta_{anis}(\nu_{15})$
0.2	2.16 (0.14) [2.22]	3.16 (0.01) [3.19]	4.10 (0.10) [4.09]	9.6 (0.1) [9.41]	9.1 (1.2) [9.93]	1.09 (0.10) [1.03]	4.28 (0.24) [4.20]	19.5 (2.2) [18.56]
0.3	2.19 (0.06) [2.40]	3.25 (0.02) [3.25]	4.21 (0.03) [4.22]	9.3 (0.3) [9.23]	10.0 (0.8) [10.40]	1.05 (0.14) [1.20]	3.62 (0.16) [4.08]	18.7 (0.5) [19.01]
0.4	2.77 (0.01) [2.58]	3.33 (0.02) [3.31]	4.38 (0.09) [4.36]	9.0 (0.9) [9.05]	12.5 (1.9) [10.9]	1.30 (0.01) [1.37]	4.36 (0.49) [3.96]	18.8 (0.7) [19.46]
0.5	2.92 (0.09) [2.76]	3.40 (0.02) [3.37]	4.50 (0.01) [4.49]	8.9 (0.2) [8.87]	12.2 (0.4) [11.34]	1.19 (0.05) [1.53]	4.25 (0.07) [3.84]	18.9 (0.4) [19.92]
0.6	3.05 (0.01) [2.94]	3.46 (0.02) [3.43]	4.65 (0.07) [4.63]	8.6 (0.2) [8.69]	10.4 (1.0) [11.81]	2.50 (0.15) [1.70]	3.63 (0.33) [3.72]	21.6 (0.4) [20.37]
0.7	3.07 (0.02) [3.12]	3.48 (0.01) [3.50]	4.81 (0.06) [4.76]	8.4 (0.4) [8.51]	12.9 (0.3) [12.29]	1.95 (0.03) [1.87]	3.44 (0.05) [3.60]	20.0 (0.9) [20.82]
0.8	3.17 (0.06) [3.29]	3.54 (0.02) [3.56]	4.90 (0.01) [4.90]	8.4 (0.2) [8.33]	12.2 (0.8) [12.76]	1.66 (0.05) [2.04]	3.39 (0.36) [3.47]	22.0 (0.5) [21.27]

a) The linewidths (FWHM) are given in units of cm^{-1}.
b) Results are the average of three measurements.
c) Quantities in parentheses are the mean deviations between runs
d) Quantities in square brackets are values obtained from a linear fit to the experimental data

B. Experimental

1. Sample Preparation

HFB and benzene were used as received without further purification. The HFB/benzene solutions were prepared gravimetrically and contained in sealed melting point capillaries. The composition of hexafluorobenzene (X_{HFB}) varied from 0.2 to 0.8 mole fraction.

2. Raman Spectrometer Measurement

The vibrations of HFB and benzene used in this investigation are listed in Table X.

Polarized Raman spectra of a_{1g} and e_{2g} modes of HFB and benzene were recorded three times at frequency increments of 0.5 cm^{-1} with a count time of 5 seconds per point. The spectroscopic width was 4.3 cm^{-1}. The depolarized spectra of these bands were also acquired for all the samples. The depolarized/polarized height and width ratios were used to correct and obtain isotropic bandwidths, Δ_{iso}, from the measured polarized widths. The Raman spectrum of each vibration was measured three times in each mixture. The experiments were performed at ambient temperature (21°C).

3. Data Analysis

The experimental spectral intensities were fitted with theoretical lorentzian lineshapes (convoluted with a triangular slit function to eliminate the effects of instrumental linebroadening) to obtain bandwidths.

In order to minimize the propagation of random error,

the widths of each vibration were fitted by a straight line and the least-square interpolated values were used in further calculations. The Raman bandwidths of a_{1g} and e_{2g} modes in HFB/Benzene solution as a function of the HFB molar fraction are listed in Table XI.

The values of $D_\perp$ were obtained from the Raman bandwidths of a_{1g} vibrations, $\Delta_{iso}(\nu_2)$ and $\Delta_{aniso}(\nu_2)$, via equation (92). The acquisition of these values and the values of $\Delta_{iso}(\nu_1)$ and $\Delta_{aniso}(\nu_{15})$ allow us to calculate the spinning diffusion coefficients, $D_\parallel$'s via equation (96). The resultant diffusion coefficients for both HFB and benzene are listed in Table XII and in Figure 9.

C. Results and Discusssion

It is observed that $D_\perp(B)$ decreases by more than a factor of two with increasing HFB mole fraction, which is in qualitative agreement with the prediction based on increasing solution viscosity,[9] as shown in Figure 9 and Table XII.

Based on hydrodynamic theories, as one may expect, the reorientational diffusion rate is proportional to $1/\eta$ ($D_\perp \propto 1/\eta$).[10] In disagreement with hydrodynamic theories of reorientation, the tumbling rate of HFB molecules, $D_\perp(HFB)$, increases with increasing solution viscosity. $D_\perp(B)$ decreases with increased solution viscosity, in agreement with the prediction of hydrodynamic theories of rotation.

Table XII. Rotational Diffusion Coefficients in Hexafluorobenzene/Benzene Mixtures[a]

X_{HFB}	$D_{\perp}$(HFB)	$D_{\perp}$(B)	$D_{\parallel}$(HFB)	$D_{\parallel}$(B)	η
0.0	--	66[b] 91[c]	-- --	216[c]	0.60
0.2	14.0	49.4	179	201	0.59
0.3	15.2	44.9	172	201	0.61
0.4	16.3	40.4	164	200	0.64
0.5	17.5	35.9	156	200	0.68
0.6	18.6	31.4	149	199	0.73
0.7	19.8	26.9	141	199	0.78
0.8	20.9	22.4	134	198	0.82
1.0	22.3[d]	--	107[d]	--	0.87

a) Diffusion coefficients given in units of ns^{-1}
b) From Ref. [7]
c) C_6H_6 in C_6D_6; K. Tanabe and J. Hiraishi, *Mol. Phys.* 39, 493 (1980)
d) From Ref. [10]

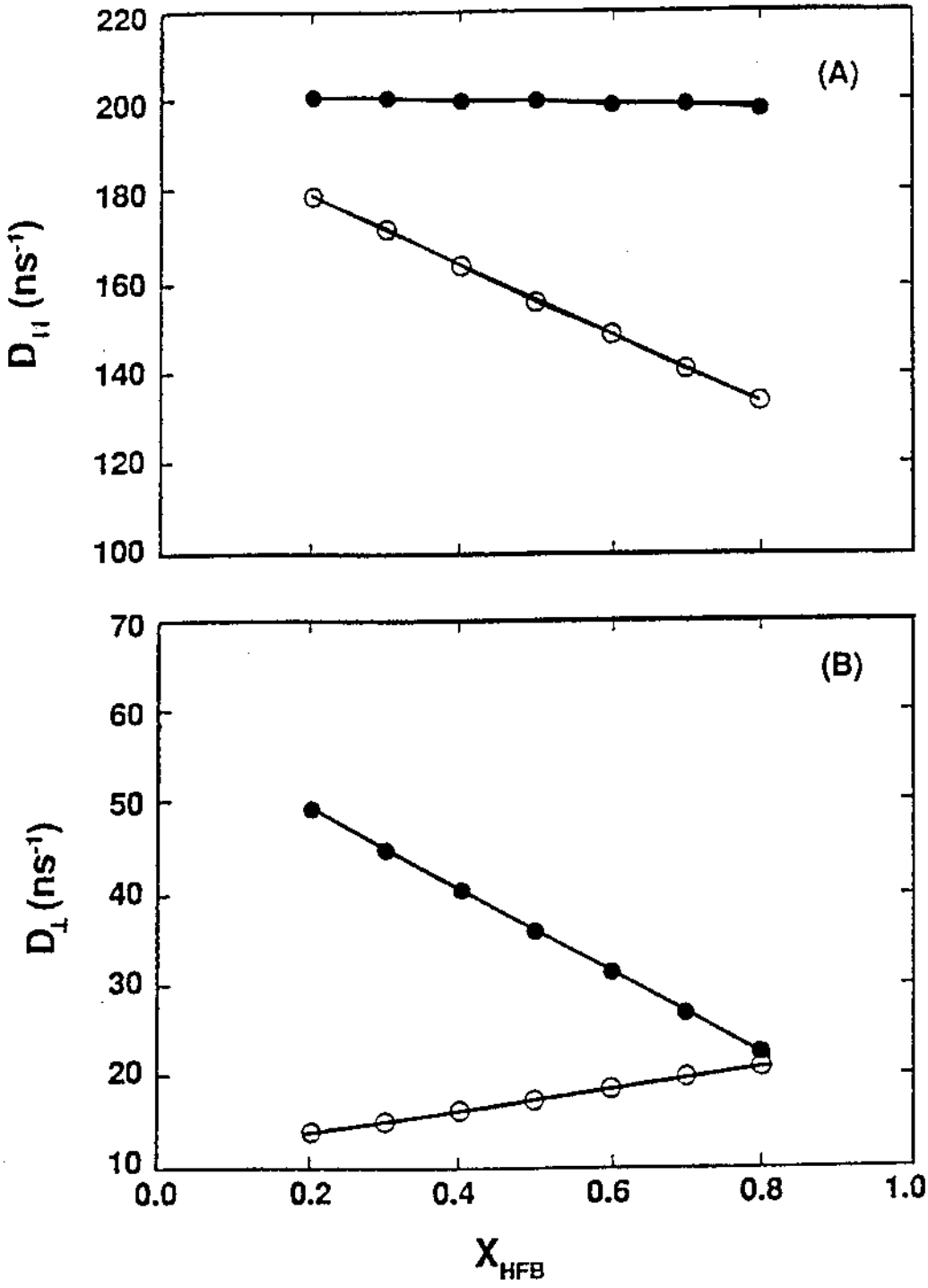

Figure 9. Composition dependence of the reorientational diffusion coefficients; Open circles - hexafluorobenzene; Close circles - benzene.
(A) $D_{||}$; (B) $D_{\perp}$.

$D_{\perp}$(HFB) exhibits a trend opposite to that of $D_{\perp}$(B), indicating that the complexation between HFB and benzene slows the tumbling rate. This phenomenon corresponds with Tanabe's finding that the formation of the associated complex tends to slow the rotation of each species as its mole fraction in the mixture is lowered.[7]

A rather different trend in the composition dependence of the parallel diffusion coefficients is found. $D_{\parallel}$(B) is roughly a constant. This implies that the benzene is spinning about the C_6 axis like a Free Rotor, which is unimpeded by varying intermolecular torques in the mixture. Also, $D_{\parallel}$(HFB) demonstrates a trend opposite to that exhibited by $D_{\perp}$(HFB), and increases at lower mole fraction of HFB. The above mentioned results imply that the relative molecular orientations are more random in neat HFB than in the mixture. In such a mixture, HFB and benzene molecules are thought to form stacked pairs.[8]

In summary, the very different trends exhibited by the perpendicular and parallel diffusion coefficients in hexafluorobenzene/benzene solution cannot be explained on the basis of a single simplified model of association and reorientation in these mixtures.

CHAPTER REFERENCES

1. (a) Patrick, C. R.; Prosser, G. S. Nature **1960**, 187, 1021.; (b) Duncan, W. A.; Swinton, F. L. Trans. Faraday Soc. **1966**, 62, 1082.

2. Bartsch, E.; Bertagnolli, H., Chieux, P.; Bunsenges, Ber. Phys. Chem. **1986**, 90, 34.

3. Gaw, W. J.; Swinton, F. L. Trans. Faraday Soc. **1968**, 64, 2023.

4. Bauer, M. E.; Horsma, D. A.; Knobler, C. M.; Peres, P. J. Chem. Phys. **1969**, 73, 641.

5. Bauer, D. R.; Brauman, J. I.; Pecora, R. J. Chem. Phys. **1975**, 63, 53.

6. Barrett, R. M.; Gill, E. B.; Steele, D. J. Chem. Soc., Faraday Trans. **1975**, 2, 71, 532.

7. Tanabe, K.; Hiraishi, J. J. Raman Spectrosc., **1982**, 12, 274.

8. Suhm, M. A.; Muller, K. J.; Weingartner, H. Zeitschrift fur Phys. Chem. Neue Folge, **1987**, 155, 101.

9. Dymond, J. H.; Robertson, J. Intl. J. Thermophys. **1985**, 6, 21.

10. Boere, R. T.; Kidd, R. G. Ann. Rep. NMR Spectrosc. **1982**, 13, 319.

BIBLIOGRAPHY

Abragam, A. Principals of Nuclear Magnetism, Oxford University Press: London, **1961**.

Barrett, R. M.; Gill, E. B.; Steele, D. J. Chem. Soc., Faraday Trans. **1975**, 2, 71, 532.

Bartoli, F. J.; Litovitz, T. A. J. Chem. Phys., **1972**, 56, 413.

Bartsch, E.; Bertagnolli, H.; Chieux, P. Ber. Bunsenges, Phys. Chem., **1986**, 90, 34.

Bauer, M. E.; Horsma, D. A.; Knobler, C. M.; Peres, P. J. Chem. Phys. **1969**, 73, 641.

Bauer, D. R.; Brauman, J. I.; Pecora, R. J. Chem. Phys. **1975**, 63, 53.

Becker, E. D. Pulse and Fourier Transform NMR, Academic: New York, **1972**; p 46.

Becker, E. D. High Resolution NMR: Theory and Chemical Applications, 2nd ed.; Academic: New York, **1980**; chapter 8, p. 188.

Becker, E. D. High Resolution NMR: Theory and Applications, 2nd ed.; Academic: New York, **1980**; Chapter 8.

Bender, H. J.; Zeidler, M.; Ber. Bunsenges. Phys. Chem. **1971**, 75, 236.

Beierbeck, H.; Martino, R. Saunders, J. K. Can. J. Chem. **1979**, 57, 1224.

Berne, B. J.; Harp, G. D. Adv. Chem. Phys., **1970**, 17, 63.

Berne, B. J. Physical Chemistry: An Advanced Treaties; Eyring, H., Henderson, D., Jost, W. ed,; Academic: New York, 1971, Vol. VIII B, p. 539.

Besnard, M.; Lascombe, J. and Nery, H. J. Phys. (paris), **1980**, 41, 723.

Bjorholm, T.; Jacobsen, J. P. Mol. Phys. **1984**, 51, 65.

Bloch, F.; Hansen, W. W.; Packard, M. E.; Phys. Rev., **1946**, 69, 127.

Bloemberg, N.; Purcell, E. M.; Pound, R. V.; Phys. Rev., **1948**, 73, 679.

Bloembergen, N.; Purcell, E. M.; Pound, R. V. Nature **1947**, 160, 475.

Boere, R. T.; Kidd, R. G. Ann. Rept. NMR Spect., **1982**, 13, 319.

Bondi, A. J. Phys. Chem. **1964**, 68, 441.

Bratos, S.; Marechal, E. Phys. Rev., **1971**, A4, 1078.

Buckro, T. A.,and Litowitz, T. A., J. Chem. Phys., **1971**, 54, 3846.

Chandra, S. and Nata, D. J. Chem. Phys. **1969**, 51, 5299.

Chen, A. F. T.; Wang, S. P.; Schwartz, M. Magn. Reson. Chem., **1988**, 26, 675.

Clarke, R. J. H. Advances in Infrared and Raman Spectroscopy; Hester, R. E. and Clarke, J. H. R., Eds.; Hyden: London, Vol. 4, **1978**; p 109.

Clarke, R. J. H. and Hester, R. E. Advances in Infrared and Raman Spectroscopy; Hyden: London, **1978**.

Craik, D. J.; Adcock, W.; Levy, G. C. Magn. Reson. Chem. **1986**, 24, 783.

Debye, P. Polar Molecules, Dover, New York, 1928.

Dewar, M. J. S.; Zoebisch, E. G.; Healy E. F.; Stewart, J. J. P. J. Amer. Chem. Soc., **1985**, 902.

Dolle, A.; Bluhm, T. Prog. NMR Spectrosc., **1989**, 21, 175.

Duncan, W. A. and Swinton, F. L. Trans. Faraday Soc. **1966**, 62, 1082.

Dymond, J. H.; Robertson, J. Intl. J. Thermophys. **1985**, 6, 21.

Edlund, U.; Holloway C. E.; Levy, G. C. J. Amer. Chem. Soc. **1976**, 98. 5069.

Emsley, J. W.; Feeney, J.; Sutcliffe, L. H.; High Resolution Nuclear Magnetic Resonance Spectroscopy, Pergamon: New York, **1965**.

Farrar, T. C.; Druck, S. J.; Shoup, P. R.; Becker, E. D.; J. Amer. Chem. Soc., **1972**, 34, 699.

Farrar, T. C. and Becker, E. D., Pulse and Fourier Transform NMR, Academic: New York, **1971**, Ch. 4.

Fischer, S. F.; Laubereau, A. Chem. Phys. Lett., **1975**, 35, 6.

Forster, D. Hydrodynamic Fluctuation, Broken Symmetry and Correlation Functions; Benjamin, **1975**.

Freeman, R.; Hill, H. D. W. Molecular Spectroscopy 1971, Institute of Petroleum, London, **1971**.

Gaw, W. J. and Swinton, F. L. Trans. Faraday Soc. **1968**, 64, 2023.

Gierer, A. Wirtz, K. Zeit. Naturforsch. **1953**, A8, 523.

Gleeson, J. W.; Vaughan, R. W. J. Chem. Phys., **1983**, 78, 5384.

Gompf, J.; Versmold, H.; Langer, H. Ber. Bunsenges. Phys. Chem., **1982**, 86, 1114.

Gordon, R. G. J. Chem. Phys., **1964**, 40, 1973.

Hawkes, G. E.; Elliot, J. E. J. Chem. Soc. Dalton Trans., **1984**, 279.

Hubbard, P. S. Phys. Rev. A., **1974**, 9, 481.

Hu, C.-M.; Zwanzig, R. J. Chem. Phys., **1976**, 60, 4354.

Huntress, W. T., Jr. J. Chem. Phys., **1968**, 48, 3524.

Hynes, J. T.; Kapral, R.; Weinberg, M. Chem. Phys. Lett, **1977**, 46, 463.

Hynes, J. T.; Kapral, R.; Weinberg, M. J. Chem. Phys., **1978**, 69, 2725.

Knozinger, E.; Kollhoff, H.; Wittenbeck, R. Ber. Bunsenges. Phys. Chem., **1982**, 86, 929.

Kubo, R. Lectures in Theoretical Physics; Vol. 1, Interscience, New York, **1961**, p. 120.

Kubo, R. J. Phys. Soc. Jap., **1975**, 12, 570.

Kubo, R. Rep. Prog. Phys., **1966**, 29 (Part 1), 255.

Lee H. I.; Kim, M. S. J. Raman Spectrosc. **1986**, 17, 269.

Leipert, T. K.; Noggle, J. H.; Gillen, K. T. J. Magn. Reson. **1974**, 13, 158.

Levy, G. C.; J. Chem. Soc., Chem. Commun., **1972**, 352.

Levy, G. C.; Cargioli, J. D.; Anet, F. A. L. J. Amer. Chem. Soc., **1973**, 25, 1672, and earlier papers.

Levy, G. C.; Terpstra, D. Org. Magn. Reson. **1976**, 8, 658.

Levy, G. C.; Holak, T. A.; Steigel, A. J. J. Amer. Chem. Soc., **1976**, 98, 495.

Lyeria, J. R., Jr.; Grant, D. M.; Bertrand, R. D.; J. Phys. Chem., **1971**, 75, 3967.

Mahake, H., Spiess, H. W.; J. Chem. Phys., **1974**, 61, 55.

Marsult, J. P.; Marsault-Herial, F.; Levi, G. J. Chem. Phys., **1975**, 62, 893.

Martin, M. L.; Martin, G. J.; Delpuech, J. J. Practical NMR Spectroscopy; Heyden: London, **1980**; Chapter 7.

Marchand, A. P. In Advances in Theoretically Interesting Molecules; Thummel, R. P., Ed.; JAI: Greenwich, CT; Vol. 1, **1989**, pp. 357-399.

Margenau, H.; Murphy, G. M. The Mathematics of Physics and Chemistry; Second Edition, Nostrand: Toronto, **1968**, p. 477.

Messiah, A. Quantum Mechanics I, Wiley: New York, 1958, p.p.135-138.

MOBY: Molecular Modeling on the PC, Version 1.4; Springer -Verlag: Berlin, **1991**.

Moniz, W. B.; Gutowsky, H. S. J. J. Chem. Phys. **1963**, 38, 115.

Miller, P. J.; Block, S. and Piermarini, G. J. J. Phys. Chem., **1989**, 93, 462.

Nafie, L. A.; Fanconi, B.; Penticolas, W. L. J. Chem. Phys., **1970**, 52, 1584.

Nafie, L. A.; Fanconi, B.; Penticolas, W. L. J. Chem. Phys., **1972**, 57, 3145.

Neuhaus, D.; Williamson, M. The Nuclear Overhauser Effect in Sterochemistry and Conformational Analysis; VCH Publishers, New York, **1989**.

Noggle, J. H.; Schirmer, R. E. The Nuclear Overhauser Effect; Academic Press: New York, **1971**.

Patrick, C. R.; Prosser, G. S. Nature **1960**, 187, 1021.

Perrin, E. J. Phys. Radium, **1934**, 5, 497.

Pople, J. A.; Schneider, W. G.; Bernstein, H. J.; High Resolution Nuclear Magnetic Resonance, McGraw-Hill: New York, **1959**.

Purcell, E. M.; Torrey, H. C.; Pound, R. V.; Phys. Rev., **1946**, 69, 37.

Ramsey, N. F.; Nuclear Moments, Wiley: New York, **1953**.

Reuven, A. B.; Gershon, N. D. J. Chem. Phys., **1969**, 51, 893.

Rodriguez, A. A.; Chen, A. F. T.; M. Schwartz, J. Mol. Liq. **1988**, 37, 117.

Rodriguez, A. A.; Chen, S. J. H.; Schwartz, M. J. Magn. Reson., **1987**, 74, 114.

Rose, M. E. Elementary Theory of Angular Momentum; Wiley: New York, **1957**.

Rothschild, W. G., Dynamics of Molecular Liquids, Wiley -Interscience, New York, **1984**.

Sandhu, H. S. J. Mag. Reson., **1978**, 29, 563.

Sandhu, H. S. J. Mag. Reson., **1977**, 26, 7.

Sandhu, H. S. J. Mag. Reson., **1976**, 21, 7.

Schlichter, C. P. Principles of Magnetic Resonance, Harper and Row: New York, **1963**.

Shimizu, H. J. Chem. Phys., **1962**, 37(4), 765.

Steele, W. A. Transport Phenomena in Fluids; Hanley H. J. M. ed., Marcel Dekker: New York, **1969**, Chapter 8.

Stokes, G. Trans. Gambridge Philos. Soc. **1856**, 9, 5.

Subbarao, S. N.; Sauer, E. G.; Bray, P. J. Phys. Lett. **1973**, 42A, 461.

Suchanski, W. Canepa, P. C., J. Magn. Reson. **1979**, 33, 389.

Suhm, M. A.; Muller, K. J.; Weingartner, H. Zeitschrift fur Phys. Chem. Neue Folge, **1987**, 155, 101.

Tanabe, K. Chem. Phys. Lett. **1979**, 6, 43.

Tanabe, K. Chem. Phys., **1978**, 31, 319.

Tanabe, K.; Hiraishi, J. Mol. Phys., **1980**, 39, 493.

Tanabe, K. Chem. Phys. **1978**, 38, 125.

Tanabe, K. and Hiraishi, J. J. Raman Spectrosc., **1982**, 12, 274.

Tobin, M. C.; Laser Raman Spectroscopy; Wiley, New York, **1971.**

Tsang, T.; Farrar, T. C. J. Chem. Phys., **1969**, 50, 3498.

Valiev, K. A. Opt. Spektrosk., **1962**, 13, 282.

Verderame, F. D.; Launon, J. A.; Harris, L. E.; Thomas, W. G.; Lucia, E. A. J. Chem. Phys. **1972**, 56, 2638.

Versmold, H. NATO ASI Ser., Ser. C **1984**, No. 135, 309.

Wang, S. P.; Chen, A. F. T.; Schwartz, M. Mol. Phys., **1988**, 65, 689.

Wang, M. C.; Uhlenbeck, G. E. Rev. Mod. Phys., **1945**, 17, 323.

Wang, S. P.; Yuan, P.; Schwartz, M. J. Raman Spectrosc. **1989**, 20, 339.

Wang, S. P.; Hu, W. P.; Schwartz, M.; Mol. Phys. **1989**, 68, 1125.

Wang, S. P.; Schwartz, M.; J. Phys. Chem. **1990**, 94, 2702.

Wasylishen, R. E.; Pettitt, B. A.; Danchura, W. Canad. J. Chem., **1977**, 55, 3602.

Watson, W. H.; Nagl, A.; Marchand, A. P.; Vidyasagar, V. Acta Crystallogr., Sect. C: Cryst. Struct. Commun. **1989**, C45, 1770.

Wilson, E. B.; J. C. Decius; P. C. Cross, Molecular Vibrations, McGraw-Hill, New York, **1955**.

Woessner, D. E. J. Chem. Phys. **1962**, 37, 647.

Wright, D. A.; Axelson, D. E.; Levy, G. C. in Topics in Carbon-1 3NMR; Levy, G. C. Ed.; Wiley: New York, **1979**; Vol. 3, p. 103.

Youngren, G. K.; Acrivos, A. J. Chem. Phys. **1975**, 63, 3846.

Yuan, P.; Schwartz, M. J. Chem. Soc., Farady Trans. **1990**, 86, 593.

Yuan, P.; Chen, A. F. T.; Schwartz, M. J. Raman Spectrosc., **1989**, 20, 27.

Zwanzig, R. Ann. Rev. Phys. Chem., **1965**, 16, 67.